

Secreted metabolome of porcine blastocysts encapsulated within *in vitro* 3D alginate hydrogel culture systems undergoing morphological changes provides insights into specific mechanisms involved in the initiation of porcine conceptus elongation

Sophie C. Walsh^A, Jeremy R. Miles^{B,*} , Corey D. Broeckling^C , Lea A. Rempel^B ,
Elane C. Wright-Johnson^B and Angela K. Pannier^{A,*} 

For full list of author affiliations and declarations see end of paper

*Correspondence to:

Jeremy R. Miles
USDA, U.S. Meat Animal Research Center,
P.O. Box 166, Clay Center, NE 68933, USA
Email: jeremy.miles@usda.gov;
Angela K. Pannier
Department of Biological Systems
Engineering, University of Nebraska-Lincoln,
P.O. Box 830726, Lincoln, NE 68583, USA
Email: apannier2@unl.edu

Handling Editor:

Ryan Cabot

Received: 21 September 2022

Accepted: 24 January 2023

Published: 14 February 2023

Cite this:

Walsh SC *et al.* (2023)
Reproduction, Fertility and Development, **35**(5),
375–394.
doi:[10.1071/RD22210](https://doi.org/10.1071/RD22210)

© 2023 The Author(s) (or their employer(s)). Published by CSIRO Publishing.
This is an open access article distributed under the Creative Commons Attribution-NonCommercial-NoDerivatives 4.0 International License (CC BY-NC-ND).

OPEN ACCESS

ABSTRACT

Context. The exact mechanisms regulating the initiation of porcine conceptus elongation are not known due to the complexity of the uterine environment. **Aims.** To identify contributing factors for initiation of conceptus elongation *in vitro*, this study evaluated differential metabolite abundance within media following culture of blastocysts within unmodified alginate (ALG) or Arg-Gly-Asp (RGD)-modified alginate hydrogel culture systems. **Methods.** Blastocysts were harvested from pregnant gilts, encapsulated within ALG or RGD or as non-encapsulated control blastocysts (CONT), and cultured. At the termination of 96 h culture, media were separated into blastocyst media groups: non-encapsulated control blastocysts (CONT); ALG and RGD blastocysts with no morphological change (ALG– and RGD–); ALG and RGD blastocysts with morphological changes (ALG+ and RGD+) and evaluated for non-targeted metabolomic profiling by liquid chromatography (LC)–mass spectrometry (MS) techniques and gas chromatography–(GC–MS). **Key results.** Analysis of variance identified 280 (LC–MS) and 1 (GC–MS) compounds that differed ($P < 0.05$), of which 134 (LC–MS) and 1 (GC–MS) were annotated. Metabolites abundance between ALG+ vs ALG–, RGD+ vs RGD–, and RGD+ vs ALG+ were further investigated to identify potential differences in metabolic processes during the initiation of elongation. **Conclusions.** This study identified changes in phospholipid, glycosphingolipid, lipid signalling, and amino acid metabolic processes as potential RGD-independent mechanisms of elongation and identified changes in lysophosphatidylcholine and sphingolipid secretions during RGD-mediated elongation. **Implications.** These results illustrate changes in phospholipid and sphingolipid metabolic processes and secretions may act as mediators of the RGD-integrin adhesion that promotes porcine conceptus elongation.

Keywords: alginate hydrogel, conceptus elongation, culture media, *in vitro*, metabolome, phospholipid, porcine, RGD, sphingolipid.

Introduction

Porcine reproductive loss occurs at a high overall percentage (~42% ova not surviving gestation per ova ovulated) (Vinsky *et al.* 2006; PigCHAMP 2020) with the majority being early embryonic and fetal mortality (Bazer *et al.* 1988; Pope 1994). Early embryonic mortality has been associated with multiple factors including improper maternal–conceptus signalling due to incompatible conceptus and endometrial development, failure of conceptus signalling, and embryonic competition for nutrients (Geisert and Schmitt 2002), which is primarily influenced by deficiencies in conceptus elongation (Pope 1994; Ashworth *et al.* 1997; Miles *et al.* 2008). The process of elongation in the

pig is characterised by a rapid and dramatic morphological change of the conceptus between days 9 and 12 of gestation from a spherical (~1–2 mm), through ovoid (~4–5 mm) and tubular (>10 mm), to a long, thin filamentous morphology (>100 mm) (Bazer *et al.* 1982; Geisert *et al.* 1982; Pope and First 1985; Miles *et al.* 2008). The events occurring during conceptus elongation that are critical to the success of the ensuing pregnancy take place within this short window of time.

The preimplantation period of conceptus development involves extensive crosstalk between the maternal endometrium and the conceptus, resulting in the induction of factors essential to survival and elongation of the conceptus, through changes in gene expression and secretion of molecular factors from both the uterine endometrium and developing conceptus (Waclawik *et al.* 2017). Although previous studies have identified increased secretion and expression of certain conceptus- and maternally-derived molecular factors and corresponding genes at the uterine–conceptus interface that influence porcine conceptus elongation (Yelich *et al.* 1997; Blomberg *et al.* 2005; Bazer and Johnson 2014; Geisert *et al.* 2014; Kiewisz *et al.* 2014), the specific mechanisms by which this process takes place remain largely unknown. Recently, our group utilised non-targeted metabolomics profiling to characterise changes in metabolite abundance within the uterine luminal fluid (ULF) of pregnant gilts as the porcine conceptus progresses through the initial morphological stages of elongation *in vivo* in order to identify novel biomarkers with potential roles in the initiation of elongation (Walsh *et al.* 2020). Additionally, we performed a global transcriptome analysis using RNA sequencing (RNA-Seq) and bioinformatic analysis to characterise changes in gene expression within the porcine conceptus as it transitions through these initial morphological stages of elongation *in vivo*, thus identifying potential mechanisms of gene regulation driving the initiation of elongation (Walsh *et al.* 2022). Together, these studies revealed new insights into mechanisms contributing to the initiation of porcine conceptus elongation, including changes in amino acid, bile, protein, purine, and energy metabolism (Walsh *et al.* 2020), as well as regulation of phospholipid membrane remodelling, lipid signalling pathways, and extracellular matrix (ECM) adhesion and remodelling (Walsh *et al.* 2022). Although these studies provide valuable insights into factors likely having the greatest influence on the initiation of porcine conceptus elongation, the complexity of the *in vivo* uterine environment and multitude of biological processes occurring during this period of gestation, as well as lack of experimental control, make it difficult to fully elucidate specific mechanisms of interest that may be essential to successful instances of elongation. Therefore, complementary studies investigating elongation of blastocysts cultured individually *in vitro* offer the ability to identify changes in distinct conceptus-derived factors that occur due to the initiation of conceptus morphological changes, as well as to directly

measure specific effects on elongation caused by the addition of individual factors to the culture.

Traditional two-dimensional (2D) cultures of preimplantation pig blastocysts do not develop through or past the stages of elongation due to loss of appropriate conceptus architecture and essential cell-to-cell communication from lack of surrounding mechanical support (Brandão *et al.* 2004). Our group has developed a three-dimensional (3D) hydrogel culture system using alginate hydrogels that facilitates the initiation of porcine conceptus elongation *in vitro*, enabling the real-time study of this process in a controlled environment (Miles *et al.* 2008, 2017; Sargus-Patino *et al.* 2014; Laughlin *et al.* 2017). Alginate is used as a synthetic matrix to completely encapsulate blastocysts via ionic crosslinking, has been shown to consistently encapsulate spherical blastocysts (~1–2 mm) harvested from gilts at day 9 of gestation, and promote blastocyst morphological change and concomitant gene expression and estradiol-17 β (E2) production consistent with the initiation of elongation *in vivo* (Sargus-Patino *et al.* 2014; Laughlin *et al.* 2017). In addition, the Arg–Gly–Asp (RGD) adhesion peptide can be covalently conjugated to the alginate matrix of the system (RGD-alginate) to model the RGD ligand-integrin receptor binding mechanism of secreted phosphoprotein 1 (SPP1) that facilitates porcine conceptus elongation and attachment to the luminal epithelium (Laughlin *et al.* 2017). This RGD modification has been shown to increase survival of encapsulated blastocysts compared to non-encapsulated, 2D control blastocysts, and increase the number of surviving blastocysts undergoing morphological change compared to blastocysts in the unmodified alginate system (ALG), presumably due to increased blastocyst-hydrogel matrix adhesion and cell migration via the stimulation of integrin signalling (Laughlin *et al.* 2017). As a result, these 3D hydrogel culture systems can provide a platform for *in vitro* study of porcine conceptus elongation that enables examination of specific porcine blastocyst characteristics attributable to changes in conceptus morphology and provides control to form hypotheses concerning the roles and mechanisms of *in vivo* influencing factors that regulate initiation of elongation.

Given the ability to individually culture blastocysts within our 3D hydrogel systems and follow their development, combined with the ability to gain mechanistic insights through understanding of metabolites secreted from a single origin (i.e. cultured blastocyst), the objective of this work was to examine differences in metabolite abundance within media, and thus corresponding to metabolite secretion of individual blastocysts either initiating or not initiating morphological changes within the culture systems, as well as a function of specific hydrogel system (i.e. ALG vs RGD-alginate). Altogether, metabolomic differences of cultured blastocysts as a function of hydrogel components and fate of blastocysts to initiate elongation *in vitro* will be evaluated and compared from these systems to develop a more detailed

understanding of the factors and mechanisms essential for initiating porcine conceptus elongation.

Materials and methods

Animal and blastocyst collection

All animal protocols were approved by the U.S. Meat Animal Research Center (USMARC) Institutional Animal Care and Use Committee (EO 65.0). Procedures for handling animals complied with the Guide for the Care and Use of Agricultural Animals in Research and Teaching (FASS 2010). Post-pubertal White crossbred gilts consisting of Landrace, Yorkshire and Duroc genetics were checked daily for oestrus. Following the first detection of oestrus (designated as day 0), gilts were artificially inseminated with semen from pooled terminal Duroc sires collected from a commercial boar stud and again 24 h later with the same pool of semen. Over a 6-month collection period, 26 pregnant gilts from six replicate collections were harvested at the USMARC abattoir on day 9 of gestation. Immediately after the gilts had been harvested, their reproductive tracts were removed and each uterine horn was flushed with 20 mL of 25 mM 4-(2-hydroxyethyl)-1-piperazineethanesulfonic acid (HEPES)-buffered Roswell Park Memorial Institute (RPMI)-1640 medium (Thermo Fisher Scientific, Waltham, MA, USA; $\sim 37^{\circ}\text{C}$) containing 1 \times antibiotics/antimycotics (Millipore Sigma, St. Louis, MO, USA). Blastocysts were recovered and classified according to morphology and size using a standard stereomicroscope (Nikon Instruments, Melville, NY, USA). Blastocysts were then washed with RPMI-1640 medium containing 1 \times antibiotics/antimycotics and 10% heat-inactivated fetal bovine serum (FBS; Invitrogen, Carlsbad, CA, USA) that had been equilibrated with 5% CO_2 . Spherical blastocysts (~ 1 mm in diameter) were randomly assigned to culture treatments for encapsulation or use as non-encapsulated control blastocysts.

Preparation of unmodified alginate and RGD-alginate solutions for blastocyst encapsulation

Unmodified alginate and RGD-alginate solutions were prepared for hydrogel encapsulation of blastocysts prior to culture following previous reported procedures (Sargus-Patino *et al.* 2014; Laughlin *et al.* 2017). For preparation of unmodified alginate, sodium alginate (Pronova UP MVG; >60% guluronic acid, 200 000–300 000 g mol^{-1} ; NovaMatrix, Sandvika, Norway) was dissolved in sterile 1 \times phosphate-buffered saline (PBS; Millipore Sigma) to a final concentration of 0.7% (w/v). For preparation of RGD-alginate, alginate was covalently modified with a Gly–Arg–Gly–Asp–Ser–Pro (GRGDSP) peptide (AnaSpec, Fremont, CA, USA) to a concentration of 3.2 $\mu\text{mol g}^{-1}$ alginate using carbodiimide chemistry, as described and characterised previously

(Rowley *et al.* 1999; Laughlin *et al.* 2017). Briefly, 2 g of sodium alginate was added to 200 mL of 4-morpholinoethane sulphonic acid (MES) buffer (0.1 M MES, 0.3 M NaCl, pH 6.5) and the alginate was allowed to dissolve for 7–8 h on a stir plate. 1-Ethyl-(dimethylaminopropyl) carbodiimide (EDC; Millipore Sigma) was added at a concentration of 250 $\mu\text{mol g}^{-1}$ alginate to activate 5% of the uronic acids of the alginate polymer backbone in order to form amide linkages with the peptide. To stabilise the reactive EDC intermediate against a competing hydrolysis reaction, *N*-hydroxy-sulphosuccinimide (sulpho-NHS; Pierce, Waltham, MA, USA) was also added at a concentration of 150 $\mu\text{mol g}^{-1}$ alginate to the solution at a ratio of 2:1 EDC to NHS. Finally, the GRGDSP peptide was incorporated at a concentration of 4 $\mu\text{mol g}^{-1}$ alginate into the solution, conjugating to the alginate backbone via the terminal amine of the peptide with a previously-reported 80% estimated efficiency (Rowley *et al.* 1999). After 20 h, the conjugation reaction was quenched by the addition of hydroxylamine hydrochloride (Millipore Sigma) at a concentration of 500 $\mu\text{mol g}^{-1}$ alginate. The alginate solution was then dialysed (3.5 kDa molecular weight cut-off, 45-mm flat-width dialysis tubing; Spectrum Laboratories, Piscataway, NJ, USA) in a salt solution (NaCl in double-distilled H_2O) with stirring over the course of 3 days. The resulting alginate solution was frozen at -80°C and lyophilised to dryness before reconstitution with PBS as described above.

Blastocyst encapsulation and culture

After the collection and washing of blastocysts, all blastocysts were placed into a Petri dish with 5% CO_2 equilibrated RPMI-1640 medium containing 1 \times antibiotics/antimycotics and 10% FBS, and were randomly assigned to one of the following three culture treatment groups, illustrated in Fig. 1 as: non-encapsulated, 2D control (CONT, $n = 51$ blastocysts); encapsulated in unmodified alginate hydrogels (ALG, $n = 101$ blastocysts); or encapsulated in RGD-alginate hydrogels (RGD, $n = 119$ blastocysts). ALG and RGD blastocysts were encapsulated within their respective alginate hydrogel using a double-encapsulation method described previously (Sargus-Patino *et al.* 2014; Laughlin *et al.* 2017). Briefly, 35- μL droplets of warmed, sterile unmodified or RGD-modified alginate solutions were placed onto polystyrene culture dishes. A single blastocyst was pipetted into each droplet of alginate in a minimal amount of the medium. Each droplet was then pipetted into a warmed, sterile crosslinking solution (50 mM CaCl_2 , 140 mM NaCl) and allowed to gel for 3 min.

The resulting alginate beads with encapsulated blastocysts were then rinsed twice in HEPES-buffered RPMI-1640 medium containing 1 \times antibiotics/antimycotics. To ensure thorough encapsulation of the blastocyst, each bead was encapsulated in a second layer of alginate, using identical methods as described above, with the exception that 50 μL

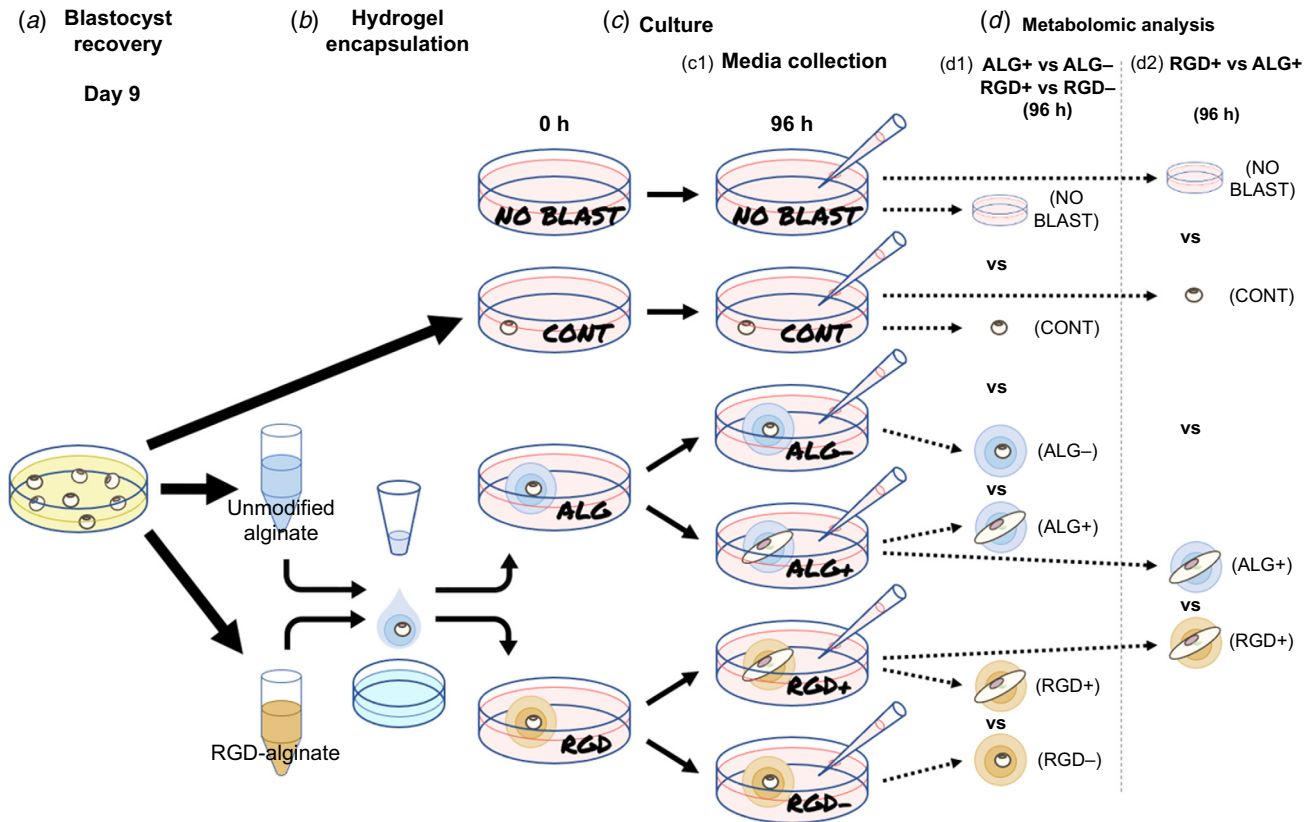


Fig. 1. Blastocyst media groups from porcine blastocysts cultured within unmodified alginate and RGD-alginate hydrogel systems analysed using non-targeted metabolomics to examine differences in metabolites secreted into culture media by porcine blastocysts initiating elongation *in vitro*. To identify metabolites specific to culture media of porcine blastocysts initiating elongation *in vitro*, (a) spherical blastocysts were harvested from pregnant gilts on day 9 of gestation. (b) Randomly assigned individual blastocysts were double-encapsulated within 3D hydrogel systems of unmodified alginate (ALG) or RGD-alginate (RGD). ALG, RGD, non-encapsulated, 2D culture control blastocysts (CONT), and media without blastocysts (NO BLAST) were (c) cultured for 96 h. (c1) Media samples (1000 μ L) were collected from NO BLAST, CONT, ALG, and RGD for metabolomic analysis at the termination of culture (96 h) and classified into six blastocyst media groups based on culture treatment and morphological change of the conceptus present: media without cultured blastocysts (NO BLAST, $n = 6$ samples); media from non-encapsulated control blastocysts (CONT, $n = 8$ blastocysts); media from ALG blastocysts with no observable morphological change (ALG-, $n = 8$ blastocysts); media from ALG blastocysts with observable morphological changes (ALG+, $n = 8$ blastocysts); media from RGD blastocysts with no observable morphological change (RGD-, $n = 8$ blastocysts); and media from RGD blastocysts with observable morphological changes (RGD+, $n = 8$ blastocysts). (d) Culture media samples were analysed using non-targeted metabolomics by both LC-MS and GC-MS to determine metabolites differing in abundance (d1) between conceptus endpoint morphologies within each hydrogel system (ALG+ vs ALG- and RGD+ vs RGD-), CONT, and NO BLAST, as well as (d2) between alginate hydrogel systems containing blastocysts initiating elongation (RGD+ vs ALG+), CONT, and NO BLAST. GC, gas chromatography; LC, liquid chromatography; MS, mass spectrometry; RGD, Arg-Gly-Asp.

of alginate was used as the base droplet to completely submerge the initial bead. The final resulting double-layered beads, along with the CONT blastocysts, were then washed once with pre-gassed (5% CO₂ in air) culture medium consisting of RPMI-1640, 1 \times antibiotics/antimycotics and 10% FBS. The CONT blastocysts, ALG blastocysts, and RGD blastocysts as well as media without blastocysts (NO BLAST), were cultured in individual wells of four-well Nunc plates (Thermo Fisher Scientific) with 1 mL of culture medium for 96 h at 38.5°C and 5% CO₂ in air with 100% humidity.

Blastocyst characterisation, sample collection, and sample preparation

At the termination of culture (96 h), an image was recorded of each blastocyst using an SMZ1500 stereomicroscope (Nikon Instruments) and the entire culture media (~1 mL) was collected, centrifuged at 2100g to remove cellular debris, and stored separately at -80°C until liquid chromatography-mass spectrometry (LC-MS) or gas chromatography (GC)-MS analysis. Blastocyst survival was determined by assessing blastocyst fragmentation (Sargus-Patino *et al.* 2014;

Laughlin *et al.* 2017). Surviving blastocysts were characterised as those with no apparent sign of cellular degeneration and dying blastocysts had significant cellular degeneration resulting in blastocyst compaction and darkening of the blastocyst. Blastocysts undergoing morphological changes were characterised by a tubular formation of the blastocyst within the gel and subsequent flattening of this tube (Sargus-Patino *et al.* 2014; Laughlin *et al.* 2017). Based on culture treatment and visual appraisal of conceptus morphological changes from blastocyst images after 96 h of culture, corresponding culture media samples of surviving blastocysts were classified into blastocyst media groups ($n = 8$ blastocysts per media group), illustrated in Fig. 1 as: media without cultured blastocysts (NO BLAST); media from non-encapsulated control blastocysts (CONT), none of which exhibited any morphological change and thus did not warrant further classification; media from ALG blastocysts with no observable morphological change (ALG-); media from ALG blastocysts with observable morphological changes (ALG+); media from RGD blastocysts with no observable morphological change (RGD-); or media from RGD blastocysts with observable morphological changes (RGD+). For metabolomic evaluations, an aliquot of each media sample (100 μ L) was placed in a 1.6-mL epitube, and 400 μ L of ice-cold 100% methanol was added. The mixture was vortexed briefly and sonicated in ice for 30 min. After sonication, the mixture was incubated at -20°C overnight (12 h) and centrifuged at 17 000g at 4°C for 15 min, and 350 μ L of the clear supernatant was collected. A 50 μ L aliquot of each sample was pooled to make a quality control (QC) sample.

LC-MS data acquisition

Extracts were injected (5 μ L) onto a Waters Acquity UPLC system (Waters Corporation, Milford, MA, USA) in randomised order with a pooled QC injection after every six samples. Separation was achieved using a Waters Acquity UPLC CSH Phenyl Hexyl column (1.7 μ M, 1.0 mm \times 100 mm), using a gradient from solvent A (water, 0.1% ammonium formate) to solvent B (acetonitrile, 0.1% formic acid). Injections were made in 99% A, held at 99% A for 1 min, ramped to 98% B over 12 min, held at 98% B for 3 min, and then returned to starting conditions over 0.05 min and allowed to re-equilibrate for 3.95 min, with a 200 μ L min^{-1} constant flow rate. The column and samples were held at 65°C and 6°C , respectively. The column eluent was infused into a Waters Xevo G2-XS Q-ToF-MS with an electrospray source in positive mode, scanning 50–1200 m/z at 0.1 s per scan, alternating between MS (6 V collision energy) and MSE mode (15–30 V ramp). Calibration was performed using sodium formate with 1 ppm mass accuracy. The capillary voltage was held at 700 V, source temperature at 150°C , and nitrogen desolvation temperature at 600°C with a flow rate of 1000 L h^{-1} .

LC-MS data processing

XCMS (v3.9.3) in R (ver. 4.0.3 (2020-10-10)) was used for feature finding, retention time alignment, correspondence analysis, and peak filling (Smith *et al.* 2006; Tautenhahn *et al.* 2008). XCMS steps included peak detection using the CentWave algorithm (ppm: 19, peakwidth: 3, 15, snthresh: 10), peak grouping with peakDensity (bw: 3, minFraction: 0.35, minSamples: 1, binSize: 0.016), retention time correction using peakDensity (minFraction: 0.5, extraPeaks: 1, smooth: loess, span: 0.2), peak regrouping using corrected retention times with peakDensity (bw: 1.2, minFraction: 0.35, minSamples: 1, binSize: 0.016), and finally peak filling using FillChromPeaks.

RAMClustR (ver. 1.1.0) in R (ver. 4.0.2) was used to normalise, filter, and group features into spectra. XCMS output data was transferred to a ramclustR object using the rc.get.xcms.data function. Feature data was extracted using the XCMS featureValues function. Features that failed to demonstrate signal intensity of at least five-fold greater in QC samples than in blanks were removed from the feature dataset (20 327 of 60 671 features were removed). Features with missing values were replaced with small values simulating noise. For each feature, the minimum detected value was multiplied by 0.1. Noise was then added using a factor of 0.1. Features were normalised by linearly regressing run order vs QC feature intensities to account for instrument signal intensity drift. Only features with a regression P -value less than 0.05 and an r -squared greater than 0.3 were corrected (27 699 of 40 344 features were corrected for run order effects). Features were filtered based on their QC sample coefficient of variation (CV) values. Only features with CV values less than or equal to 0.5 in MS or MSMS datasets were retained (8881 of 40 344 features were removed). Features were clustered using the ramclustR algorithm (Broeckling *et al.* 2014). Parameter settings were as follows: st = 3.36, sr = 0.7, maxt = 336, deepSplit = FALSE, hmax = 0.3, minModuleSize = 4, and cor.method = pearson. Molecular weight was inferred from in-source spectra (Broeckling *et al.* 2016) using the do.findmain function, which calls the interpretMSSpectrum package (Jaeger *et al.* 2017). Parameters for do.findmain were set to: mode = positive, mzabs.error = 0.005, ppm.error = 8, ads = default, scoring = auto, and use.z = TRUE. MSFinder (Tsugawa *et al.* 2016) was used for spectral matching, formula inference, and tentative structure assignment, and results were imported into the RAMClustR object.

Annotations were assigned using the RAMClustR annotate function. Annotation priority was assigned from highest priority to lowest: MSFinder structure, MSFinder formula, interpretMSSpectrum M. MSFinder structures were considered from databases including HMDB, ChEBI, Pubchem, and LipidMAPS. Database priority was set to HMDB and ChEBI. Compounds were assigned to chemical ontogenies using the ClassyFire API (Djombou Feunang *et al.* 2016).

GC–MS data acquisition

An aliquot of 80 μL of the methanol extract was dried under a stream of nitrogen. The dried extract was first derivatised with 50 μL of 25 mg mL^{-1} of methoxyamine hydrochloride in pyridine for 1.5 h at 60°C, then with 50 μL of *N*-methyl-*N*-trimethylsilyltrifluoroacetamide plus 1% trimethylchlorosilane (MSTFA + 1% TMCS; Thermo Fisher Scientific) for 0.5 h at 60°C. Analysis and detection were done with a Trace 1310 GC (Thermo Fisher Scientific) coupled to an ISQ mass spectrometer (Thermo Fisher Scientific). Samples (1 μL) were injected into an injection port at 285°C and 1:10 split ratio. Separation was accomplished with a 30 m TG-5MS column (0.25-mm i.d., 0.25- μm film thickness; Thermo Fisher Scientific) and a helium gas at 1.2 mL min^{-1} flow rate. The oven temperature program started at 80°C for 30 s, ramped to 330°C at 15°C min^{-1} , and then held at the final temperature for 8 min. The transfer line and ion source were maintained at 300°C and 260°C, respectively. Masses between 50 and 650 m/z were scanned at 5 scans s^{-1} after electron impact ionisation. A QC sample was injected after every six samples.

GC–MS data processing

RAMClustR (ver. 1.1.0) in R (ver. 4.0.3) was used to normalise, filter and group features into spectra. XCMS (Smith *et al.* 2006) output data was transferred to a ramclustR object using the `rc.get.xcms.data` function. Feature data was extracted using the XCMS `featureValues` function. Features which failed to demonstrate signal intensity of at least three-fold greater in QC samples than in blanks were removed from the feature dataset (13 321 of 29 417 features were removed). Features were filtered based on their QC sample CV values. Only features with CV values less than or equal to 0.5 in MSdata set were retained (13 000 of 16 096 features were removed). Features with missing values were replaced with small values simulating noise. For each feature, the minimum detected value was multiplied by 0.5. Noise was then added using a factor of 0.1. Features were normalised by linearly regressing run order vs QC feature intensities to account for instrument signal intensity drift. Only features with a regression *P*-value less than 0.01 and an *r*-squared greater than 0.2 were corrected (27 of 3096 features were corrected for run order effects in at least one batch). Batch effects were normalised to median intensity for each feature. Features were clustered using the ramclustR algorithm (Broeckling *et al.* 2014). Parameter settings were as follows: `st = 1.22`, `sr = 0.7`, `maxt = 122`, `deepSplit = FALSE`, `hmax = 0.3`, `minModuleSize = 2`, and `cor.method = pearson`. Annotation was performed in RAMSearch [28], and annotations imported in the ramclustR object. Annotations were assigned manually using the RAMsearch program (Broeckling *et al.* 2016), searching against the GOLM and NIST 17 EI spectral databases, then imported to R using the

RAMClustR `annotate` function. Compounds were assigned to chemical ontogenies using the ClassyFire API (Djoumbou Feunang *et al.* 2016). Pubchem data was retrieved using the PUG rest interface (Kim *et al.* 2019).

Statistical analysis

Prior to analysis, one ALG+ media sample (GC–MS) and one RGD– media sample (GC–MS) were removed from the analysis due to failing the initial QC. Principal component analysis (PCA) was performed in R and the SpecAbund dataset was used as input with scaling set to pareto. The number was selected using the AuerGervini method from the ClassDiscovery R package. The median value of all principal component values from the ‘compareAgDimMethods’ function was used to set principal components to 8 (for LC–MS data). Linear model analysis of variance (ANOVA) was performed for the factor [blastocyst media group] to provide some guidance on which principal components appear responsive to factors of interest. These were not meant to be rigorous statistical tests but to help guide interpretation of the data. ANOVA was performed in R and the SpecAbund dataset was used as input. To determine specific differences in metabolite abundance, Mixed model ANOVA was performed using the `Imer` and `ImerTest` functions and *P*-values were assigned and separated using the ‘`anova`’ function with `ddf` set to ‘Kenward-Roger.’ *P*-value correction was performed using the `p.adjust` function with method set to Benjamini-Hochburg false discovery rate (FDR) correction. Following analysis, metabolite abundances were reported as least-squared means (LSM) \pm standard error of the mean (s.e.m.) and were normalised relative to CONT (CONT values set to 1 for each metabolite) for presentation.

Results

Culture media samples were analysed using non-targeted metabolomics by both LC–MS and GC–MS to produce a metabolic profile across blastocyst media groups after 96 h of culture. Liquid chromatography–mass spectrometry analysis detected 1475 metabolic compounds (Table S1) from the media samples, while GC–MS analysis detected 505 compounds (Table S2).

Principal component analysis

Principal component analysis of both LC–MS and GC–MS datasets was performed as a multivariate tool to summarise the culture media metabolome (Fig. 2). For the LC–MS dataset, the PCA that best described the dataset-wide variance was PC1 ($P < 0.05$) and PC2 ($P < 0.05$) and explained 54% of the Pareto-scaled dataset-wide variance (Fig. 2a). The loading plot for the LC–MS dataset (Fig. 2b) demonstrated

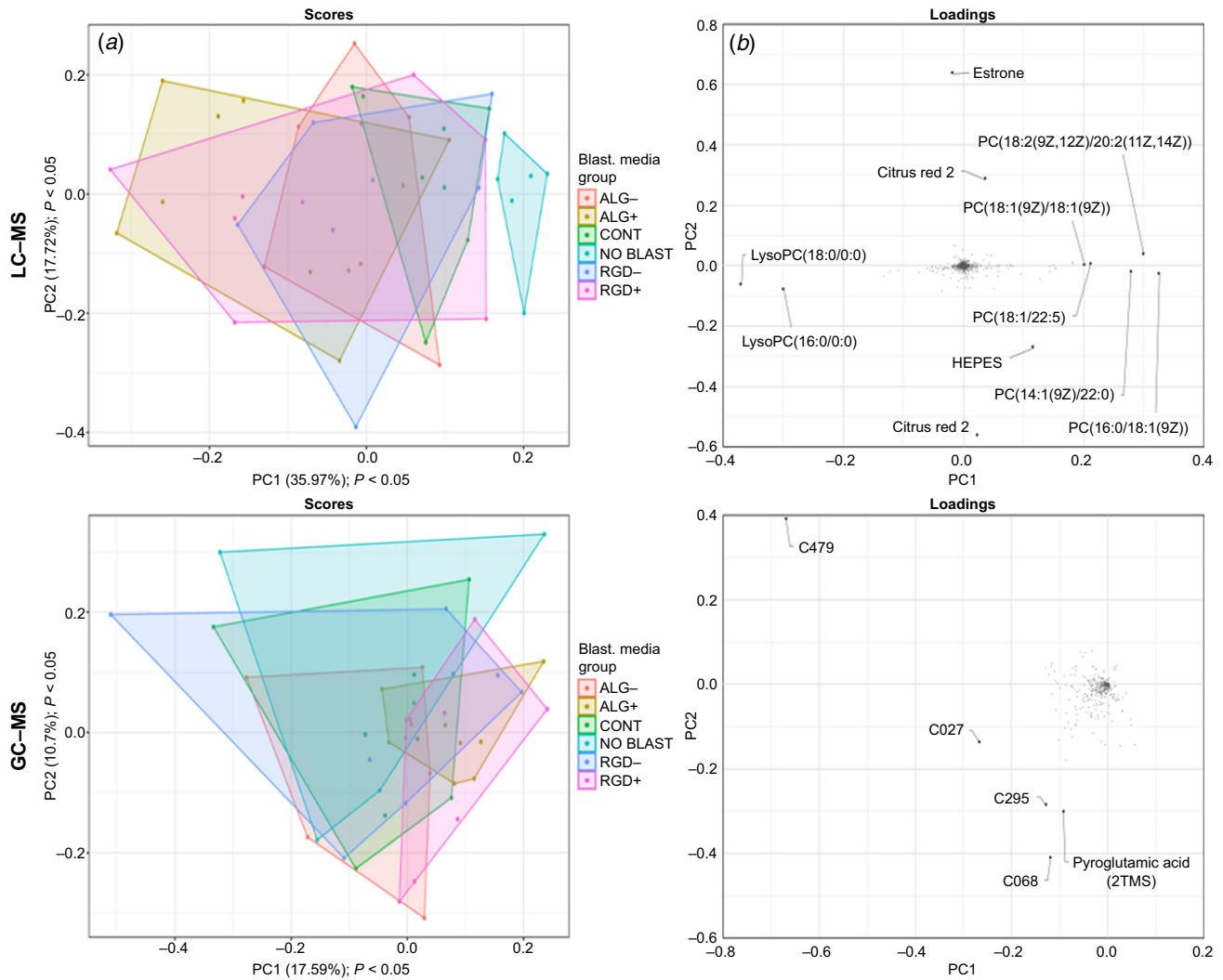


Fig. 2. PCA scores and loading plots summarising the metabolome differences between blastocyst media groups based on culture treatment and conceptus morphological change. PCA scores and loading plots (*a/c* and *b/d*, respectively); LC-MS and GC-MS datasets (*a/b* and *c/d*, respectively). (*a*) PCA scores plot for the LC-MS dataset illustrates the best separation of culture media based on culture treatment and conceptus morphological change resulted from the analysis of PC1 and PC2, which collectively explain 54% of the Pareto-scaled dataset-wide variance. (*c*) PCA scores plot for the GC-MS dataset illustrates the best separation of culture media based on culture treatment and conceptus morphological change resulted from the analysis of PC1 and PC2, which collectively explain 28% of the Pareto-scaled dataset-wide variance. (*b,d*) The loading plot on the right of the respective datasets demonstrates the weights of each individual metabolite that contributes to the separation of samples on the left scores plot. ALG-, unmodified alginate not initiating elongation; ALG+, unmodified alginate initiating elongation; CONT, non-encapsulated control; GC, gas chromatography; LC, liquid chromatography; MS, mass spectrometry; NO BLAST, media without blastocyst; PCA, principal component analysis; RGD-, RGD-alginate not initiating elongation; RGD+, RGD-alginate initiating elongation; TMS, trimethylsilyl.

the weight that each individual metabolite contributed to the separation of media samples on the PCA scores plot. The LC-MS loading plot illustrated that lysophosphatidylcholine (LysoPC) metabolites of ALG+ and RGD+ media separated the culture media of elongating blastocysts from the other groups (Fig. 2*b*). In contrast, phosphatidylcholine (PC) metabolites separated the metabolomes of CONT and NO BLAST groups to the right

of the other groups and estrone separated groups containing cultured blastocysts (i.e. CONT, ALG+, ALG-, RGD+, and RGD- media) toward the top of the scores plot (Fig. 2*b*). For the GC-MS dataset, the PCA that best described the Pareto-scaled dataset-wide variance was PC1 ($P < 0.05$) and PC2 ($P < 0.05$), collectively explained 28% of the variance (Fig. 2*c*). Pyroglutamic acid shifted the metabolomes of ALG+, ALG-, and RGD+ media toward

the bottom right of the scores for the GC-MS loading plot compared to other groups (Fig. 2d).

One-way analysis of variance

Once metabolites contributing to separation differences in culture treatment and conceptus endpoint morphology metabolomes of culture media were identified with PCA, one-way ANOVA tests with subsequent Benjamini-Hochburg FDR correction was applied to each of the 1475 and 505 compounds detected by LC-MS and GC-MS methods, respectively (Tables S1, S2). The analysis identified 280 LC-MS compounds and 1 GC-MS compound that differed ($P < 0.05$) within culture media due to culture treatment and conceptus morphological change, illustrated in Fig. 3 and reported in Table S3. Of these differing compounds, 134 LC-MS and 1 GC-MS compounds were annotated (Table S3).

Differential abundance of metabolites between blastocyst media groups that initiation elongation *in vitro* after 96 h of culture

The 134/1 (LC-MS/GC-MS, respectively) annotated compounds were subjected to the following pairwise

comparisons: (1) ALG+ vs ALG-; (2) RGD+ vs RGD-; and (3) RGD+ vs ALG+), to evaluate metabolite differences in culture media of porcine blastocysts that specifically initiated elongation *in vitro* and as a function of hydrogel system. A total of 34 LC-MS compounds differed ($P < 0.05$) and no difference for the GC-MS compound were detected between ALG+ vs ALG-, RGD+ vs RGD-, and/or RGD+ vs ALG+ (Tables 1, 2, 3). Differences in abundance of metabolites between these specific blastocyst media groups are examined individually in the following sections to provide insights into potential metabolic differences resulting from morphological changes within the different hydrogel culture systems.

Differential abundance of metabolites between media from ALG+ blastocysts and media from ALG- blastocysts (ALG+ vs ALG-)

Ten annotated LC-MS compounds differed ($P < 0.05$) between ALG+ and ALG- media (Table 1), including metabolites involved in phospholipid metabolism (i.e. LysoPC(17:0/0:0), PC(20:1/18:1), and triacylglycerol (TAG) (22:0/24:0/22:2) and glycosphingolipid metabolism [i.e. trihexosylceramide (Gb3) (d18:1/16:0)] (Fig. 4a), lipid signalling metabolism [i.e. prostanoids (prostaglandin [PG] A₂ [PGA2] and thromboxane [THX] A₂ [TXA2]) and

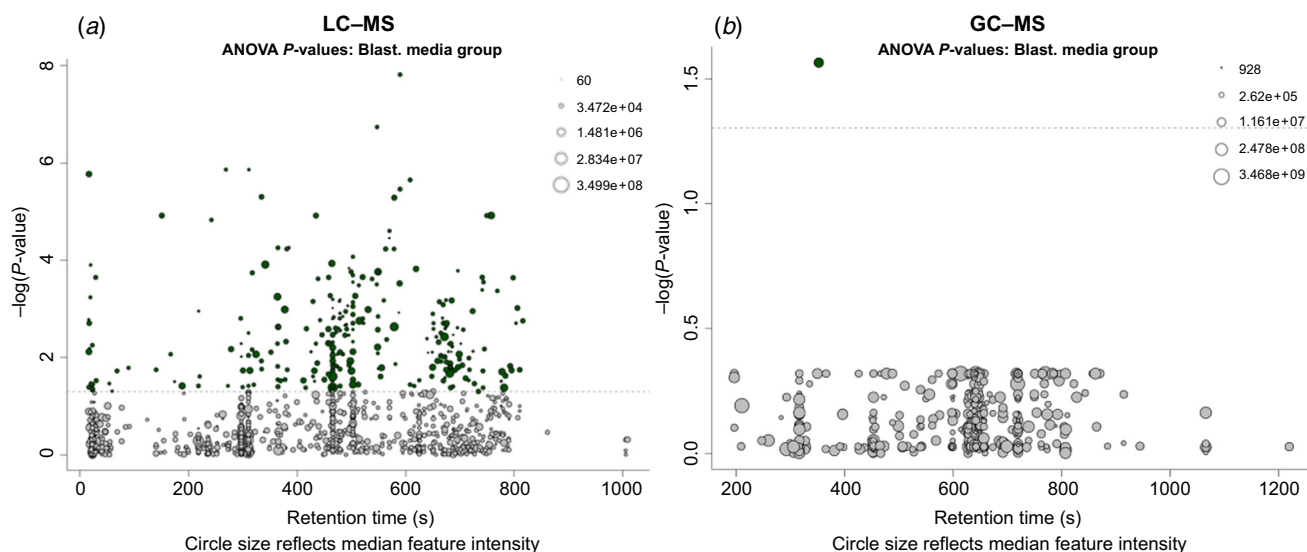


Fig. 3. ANOVA bubble plots of compounds differing ($P < 0.05$) within blastocyst media groups due to culture treatment and conceptus morphological change. (a) LC-MS and (b) GC-MS ANOVA bubble plots of compounds separating culture media by the effect of culture treatment and conceptus morphology present after 96 h of culture. This plot depicts the P -value for each metabolite and factor on the $-\log_{10}$ scale (y -axis). The x -axis represents retention time. Point size reflects the number of mass features for each compound, an approximation of signal intensity, and spectrum complexity. All coloured points above the dotted line are deemed differing in abundance based on blastocyst media group after FDR correction at $P < 0.05$ level among culture media containing one of the six blastocyst culture treatment/endpoint morphology groups (i.e. NO BLAST, CONT, ALG-, ALG+, RGD-, or RGD+). ALG-, unmodified alginate not initiating elongation; ALG+, unmodified alginate initiating elongation; ANOVA, analysis of variance; CONT, non-encapsulated control; FDR, false discovery rate; GC, gas chromatography; LC, liquid chromatography; MS, mass spectrometry; NO BLAST, media without blastocyst; RGD-, RGD-alginate not initiating elongation; RGD+, RGD-alginate initiating elongation.

Table 1. Metabolites detected by LC–MS that differed ($P < 0.05$) between media collected from blastocysts encapsulated in unmodified alginate (ALG) that initiated (ALG+) or did not initiate (ALG–) elongation after 96 h of culture.

Compound	Annotated compound	Fold change (ALG+/ALG–)	P-value	Score ^A	Retention time (s)
C0886	(R)-Salsolinol	1.709100847	0.022820433	2	150.6844
C0067	3-OH-Isobutyryl-CoA	1.195965670	0.036769514	2	502.9226944
C0437	17-OHP	2.812157866	0.035106116	2	379.6384444
C0455	Ivacaftor	1.428379512	0.012170636	2	563.2094444
C0734	LysoPC(17:0/0:0)	1.464694964	0.041676783	2	465.587
C0633	PC(20:1/18:1)	1.190909212	0.041287819	2	671.5918571
C1381	PGA2	1.915563587	0.008495187	2	381.018
C1363	TAG(22:0/24:0/22:2)	1.507190476	0.021994769	2	364.80725
C0936	TXA2	2.010669916	0.007173266	2	341.3624
C0992	Gb3(d18:1/16:0)	1.585337470	0.001695569	2	619.1668

^AAnnotation confidence score (scale of 1–4) based on guidelines provided by the Metabolomics Standards Initiative (Sumner *et al.* 2007).

3-OH-Isobutyryl-CoA, (S)-3-hydroxyisobutyryl-CoA; 17-OHP, 17-hydroxyprogesterone; Cmpnd., compound; Gb3, trihexosylceramide; LC–MS, liquid chromatography–mass spectrometry; LysoPC, lysophosphatidylcholine; PC, phosphatidylcholine; PGA2, prostaglandin A₂; TAG, triacylglycerol; TXA2, thromboxane A₂.

Table 2. Metabolites detected by LC–MS that differed ($P < 0.05$) between media collected from blastocysts encapsulated in RGD-alginate (RGD) that initiated (RGD+) or did not initiate (RGD–) elongation after 96 h of culture.

Compound	Annotated compound	Fold change (RGD+/RGD–)	P-value	Score ^A	Retention time (s)
C0644	3-Hydroxysintaxanthin	0.914032230	0.011471111	2	548.4481429
C0221	8-Methylnonenoate	0.903450461	0.007991963	2	548.8358125
C0225	LysoPC(20:3/0:0)	0.842689926	0.028742749	2	474.3332667
C0226	LysoPC(20:4/0:0)	0.816843484	0.021634656	2	461.5440667
C0514	LysoPC(20:4/0:0)	0.869292004	0.041743623	2	455.079875
C0267	LysoPC(22:4/0:0)	0.854913141	0.007339934	2	491.3725385

^AAnnotation confidence score (scale of 1–4) based on guidelines provided by the Metabolomics Standards Initiative (Sumner *et al.* 2007).

Cmpnd., compound; LC–MS, liquid chromatography–mass spectrometry; LysoPC, lysophosphatidylcholine.

17-hydroxyprogesterone (17-OHP)] (Fig. 4b), and amino acid metabolism [i.e. (R)-salsolinol and (S)-3-hydroxyisobutyryl-CoA (3-OH-isobutyryl-CoA)] (Fig. 4c). These compounds had greater ($P < 0.05$) normalised abundance in ALG+ media compared to ALG– media (Fig. 4). Specifically, PC(20:1/18:1), LysoPC(17:0/0:0), and TAG(22:0/24:0/22:2) abundance were greater ($P < 0.05$) in ALG+ media compared to all other blastocyst media groups (Fig. 4a). Similarly, the abundance of Gb3(d18:1/16:0) was greatest ($P < 0.05$) in ALG+ and RGD+ media (Fig. 4a). PGA2 and TXA2 abundance was greater ($P < 0.05$) in ALG+ media compared to all other blastocyst media groups except for the RGD+ media (Fig. 4b). The abundance of 17-OHP was increased ($P < 0.05$) in ALG+ media compared to all other media conditions aside from RGD+ media, which was intermediate (Fig. 4b). The abundance of (R)-salsolinol was greatest ($P < 0.05$) in ALG+ and RGD+ media with RGD+ having an intermediate abundance between ALG+ and both ALG– and RGD– media groups (Fig. 4c). 3-OH-Isobutyryl-CoA had greater

($P < 0.05$) abundance in ALG+ media than in the blastocyst media groups without alginate encapsulation but was not different ($P > 0.10$) from the RGD blastocyst media groups (Fig. 4c).

Differential abundance of metabolites between media from RGD+ blastocysts and media from RGD– blastocysts (RGD+ vs RGD–)

Six annotated LC–MS compounds differed ($P < 0.05$) between RGD+ and RGD– media (Table 2), including LysoPCs [i.e. LysoPC(20:3/0:0), LysoPC(20:4/0:0), LysoPC(20:4/0:0), and LysoPC(22:4/0:0)] (Fig. 5). These compounds had reduced ($P < 0.05$) abundance in RGD+ media compared to RGD– media (Fig. 5). In addition, the abundance of LysoPC(20:3/0:0), LysoPC(20:4/0:0), and LysoPC(22:4/0:0) were decreased ($P < 0.05$) in ALG+ media compared to the NO BLAST media and intermediate among the other blastocyst media groups (Fig. 5).

Table 3. Metabolites detected by LC–MS that differed ($P < 0.05$) between media collected from blastocysts initiating elongation after 96 h of culture encapsulated in RGD-alginate (RGD+) or unmodified alginate (ALG+).

Compound	Annotated compound	Fold change (RGD+/ALG+)	P-value	Score ^A	Retention time (s)
C0957	Cer(d18:0/22:0)	0.732675555	0.032938020	2	745.1954
C1409	Cer(d18:0/24:1)	0.670529661	0.001726807	2	769.02075
C0617	Cer(d18:1/20:0)	0.825111500	0.017418216	2	723.638
C1397	Cer(d18:1/22:0)	0.738320182	0.001447595	2	741.16125
C0213	Cer(d18:1/22:0)	0.833392460	0.003459730	2	741.1569375
C0964	Cer(d18:1/24:0)	0.704618320	0.000164826	2	757.7046
C0311	Cer(d18:1/24:1)	0.824494977	0.005450483	2	743.5181667
C1365	Cornudentanone	0.753612367	0.038095592	2	366.535
C0057	Exiguafavanone B	0.845966209	0.014356479	2	16.1203
C0950	LysoPC(16:1/0:0)	0.841297460	0.031479719	2	434.6974
C0511	LysoPC(17:1/0:0)	0.849981521	0.014211272	2	461.135625
C0036	LysoPC(18:1/0:0)	0.861939563	0.026015570	2	479.1620577
C0305	LysoPC(20:2/0:0)	0.863601036	0.047331791	2	493.3833333
C0127	LysoPC(22:0/0:0)	0.823053538	0.016153023	2	570.2499565
C1010	LysoPC(24:1/0:0)	0.862742998	0.034301807	2	578.64
C0104	LysoPE(0:0/22:1)	0.814526029	0.043858727	2	495.6808462
C0633	PC(20:1/18:1)	0.819319829	0.015197530	2	671.5918571
C0383	Penicillin G	0.728235523	0.004327839	2	363.915
C0217	SM(d18:1/22:0)	0.929599837	0.025341583	2	699.1699375
C1363	TAG(22:0/24:0/22:2)	0.646542119	0.014149988	2	364.80725

^AAnnotation confidence score (scale of 1–4) based on guidelines provided by the Metabolomics Standards Initiative (Sumner et al. 2007).

Cer, ceramide; Cmpnd., compound; LC–MS, liquid chromatography–mass spectrometry; LysoPC, lysophosphatidylcholine; LysoPE, lysophosphatidylethanolamine; PC, phosphatidylcholine; SM, sphingomyelin; TAG, triacylglycerol.

Differential abundance of metabolites between media from RGD+ blastocysts and media from ALG+ blastocysts (RGD+ vs ALG+)

Twenty annotated LC–MS compounds differed ($P < 0.05$) between RGD+ and ALG+ (Table 3), including metabolites involved in phospholipid metabolism [i.e. long-chain fatty acyl (LCFA) LysoPCs (LysoPC(16:1/0:0), LysoPC(17:1/0:0), LysoPC(18:1/0:0), and LysoPC(20:2/0:0) (Fig. 6a), very-LCFA (VLCFA) LysoPCs (LysoPC(22:0/0:0) and LysoPC(24:1/0:0) (Fig. 6b), and PC(20:1/18:1), lysophosphatidylethanolamine (LysoPE) (0:0/22:1), and TAG(22:0/24:0/22:2) (Fig. 6c)] and sphingolipid metabolism [i.e. ceramides (Cers) (Cer(d18:1/20:0), Cer(d18:1/22:0), Cer(d18:1/24:0), and Cer(d18:1/24:1) (Fig. 7a) and dihydroceramides (DhCers) (Cer(d18:0/22:0) and Cer(d18:0/24:1) and sphingomyelin (SM) (d18:1/22:0) (Fig. 7b)]. These compounds had decreased ($P < 0.05$) normalised abundance in RGD+ media compared to ALG+ media (Figs 6, 7).

The abundance of LysoPC(16:1/0:0), LysoPC(17:1/0:0), LysoPC(18:1/0:0), and LysoPC(20:2/0:0) was also increased ($P < 0.05$) in ALG+ media compared to NO BLAST and CONT (Fig. 6a). Additionally, LysoPC(22:0/0:0),

LysoPC(24:1/0:0), and LysoPE(0:0/22:1) abundance was greater ($P < 0.05$) in ALG+ media than in all other blastocyst media groups aside from ALG– media (Fig. 6b–c). Further, LysoPC(22:0/0:0) abundance was increased ($P < 0.05$) in all blastocyst media groups containing cultured blastocysts (i.e. CONT, ALG–, ALG+, RGD–, and RGD+ media) compared to NO BLAST, while LysoPC(24:1/0:0) and LysoPE(0:0/22:1) abundance was greater ($P < 0.05$) in media of all encapsulation blastocyst media groups (i.e. ALG–, ALG+, RGD–, and RGD+ media) compared to NO BLAST.

Additionally, abundance of Cer(d18:1/22:0) and Cer(d18:1/24:1) was increased ($P < 0.05$) in ALG blastocyst media groups (ALG+ and ALG–) compared to RGD+, RGD–, and NO BLAST media (Fig. 7a). Cer(d18:1/24:0) abundance was also increased ($P < 0.05$) in the ALG blastocyst media groups compared to all other media groups (NO BLAST, CONT, RGD+, and RGD–; Fig. 7a). Further, abundance of Cer(d18:1/20:0) and SM(d18:1/22:0) was increased ($P < 0.05$) in ALG– media compared to RGD+, RGD–, and NO BLAST media; Cer(d18:1/20:0) abundance was also greater ($P < 0.05$) in ALG+ and CONT media than NO BLAST (Fig. 7a–b). The abundance of Cer(d18:0/24:1)

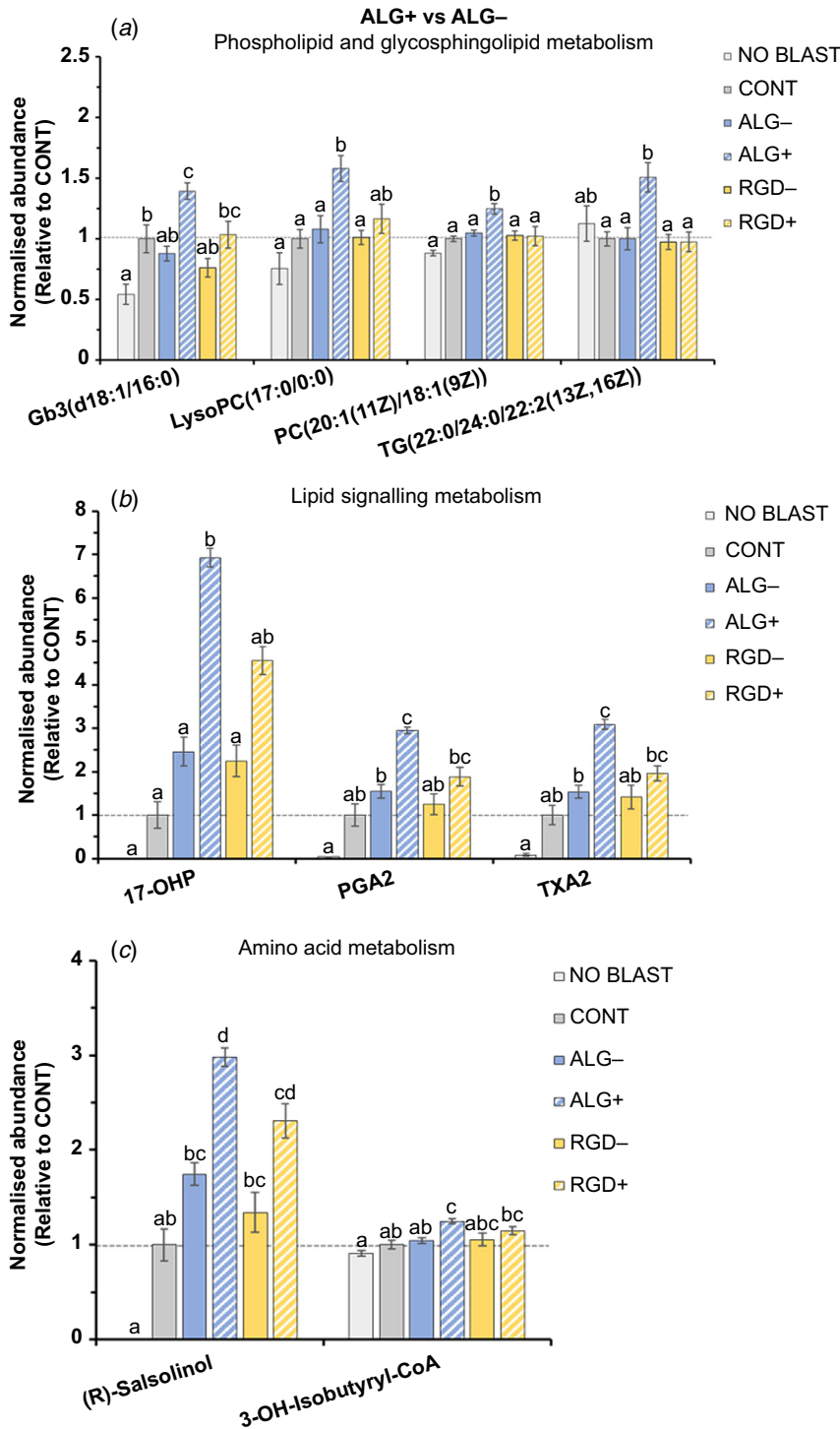


Fig. 4. Differences in metabolite abundance of media from porcine blastocysts initiating elongation *in vitro* within unmodified alginate hydrogels. Differences ($P < 0.05$) in normalised abundance of metabolites between media collected from blastocysts encapsulated in unmodified alginate (ALG) that initiated (ALG+) or did not initiate (ALG-) elongation after 96 h of culture involved in (a) phospholipid and glycosphingolipid metabolism, (b) lipid signalling metabolism, or (c) amino acid metabolism. Bar graphs depict the influence of morphological change of blastocysts encapsulated within unmodified alginate on the normalised abundance of the metabolites within corresponding culture media; graphs also display pairwise comparisons of normalised metabolite abundance within media from ALG+, ALG-, blastocysts encapsulated in RGD-alginate (RGD) that initiated elongation (RGD+), RGD blastocysts that did not initiate elongation (RGD-), non-encapsulated, 2D culture control blastocysts (CONT), and media without cultured blastocysts (NO BLAST). Metabolite abundance values are reported as LSM \pm s.e.m. and normalised relative to CONT for each metabolite (CONT values are designated as 1, indicated by the dashed line at $y = 1$); bars with different letters differ ($P < 0.05$) for each metabolite.

was increased ($P < 0.05$) in ALG+ media than in all other blastocyst media groups aside from ALG- media, which had a greater ($P < 0.05$) abundance than RGD+, RGD-, and NO BLAST media. Lastly, Cer(d18:0/22:0) abundance was greater ($P < 0.05$) in ALG+ media than in both RGD blastocyst media groups and was increased ($P < 0.05$) ALG- media than in RGD- media.

Discussion

In the current study, we characterised differences in metabolites secreted by porcine blastocysts cultured within unmodified ALG and RGD-alginate hydrogel systems that did or did not initiate morphological change after 96 h of culture. Differences in metabolite abundance between

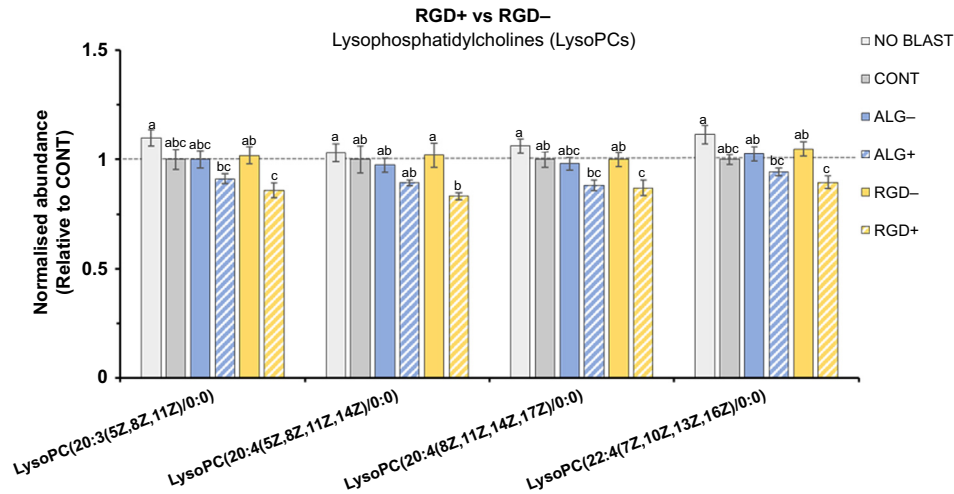


Fig. 5. Differences in metabolite abundance of media from porcine blastocysts initiating elongation *in vitro* within RGD-alginate hydrogels. Differences ($P < 0.05$) in normalised abundance of selected annotated metabolites between media collected from blastocysts encapsulated in RGD-alginate (RGD) that initiated (RGD+) or did not initiate (RGD-) elongation after 96 h of culture. Bar graph depicts the influence of morphological change of blastocysts encapsulated within RGD-alginate on the normalised abundance of the metabolites within corresponding culture media; graph also displays pairwise comparisons of normalised metabolite abundance within media from RGD+, RGD-, blastocysts encapsulated in unmodified alginate (ALG) that initiated elongation (ALG+), ALG blastocysts that did not initiate elongation (ALG-), non-encapsulated, 2D culture control blastocysts (CONT), and media without cultured blastocysts (NO BLAST). Metabolite abundance values are reported as $LSM \pm s.e.m.$ and normalised relative to CONT for each metabolite (CONT values are designated as 1, indicated by the dashed line at $y = 1$); bars with different letters differ ($P < 0.05$) for each metabolite.

blastocyst media groups illustrate potential RGD-independent as well as specific RGD-mediated mechanisms, indicating changes in the conceptus phospholipid and sphingolipid metabolic processes may regulate the initiation of porcine conceptus elongation. These metabolic differences observed in elongating porcine blastocysts encapsulated within 3D alginate hydrogel systems during culture, as well as their potential roles in the initiation of porcine conceptus elongation, are discussed separately in the following sections.

Metabolic differences between ALG+ and ALG- blastocysts after 96 h of culture

We have previously shown that spherical porcine blastocysts encapsulated within unmodified alginate hydrogel culture system that initiated morphological changes had greater abundance of transcripts for steroidogenic enzymes and E2 production and secretion, compared to encapsulated or non-encapsulated control blastocysts that did not initiate morphological change (Sargus-Patino et al. 2014), consistent with similar observed increases in transcript expression and E2 production/secretion in later-stage *in vivo*-produced blastocysts (i.e. ovoid and tubular blastocysts) that have initiated the elongation process (Blomberg et al. 2006; Miles et al. 2008; Sargus-Patino et al. 2014; Laughlin et al. 2017).

Interestingly, while expression of interleukin 1-beta (*IL1B*) was greater in elongating encapsulated blastocysts compared to non-encapsulated control blastocysts, its expression was decreased in elongating encapsulated blastocysts compared to *in vivo*-produced tubular blastocysts. Together, these results suggest that conceptus upregulation of *IL1B* during elongation requires interaction of the conceptus with the maternal endometrium and factors within the uterine milieu, whereas upregulation of steroidogenic transcripts and E2 production may occur independently of maternal-conceptus crosstalk (Sargus-Patino et al. 2014; Miles et al. 2017).

Within the current study, the abundance of phospholipid metabolites including LysoPC(17:0/0:0), PC(20:1/18:1), and TAG(22:0/24:0/22:2) was greater in media from ALG+ blastocysts than in media from ALG- blastocysts. Phosphatidylcholine (20:1/18:1) contains an eicosenoyl and oleoyl chain at the *sn*-1 and *sn*-2 position, respectively (Arnhold et al. 2002; Liebisch et al. 2013), and LysoPC(17:0/0:0) contains a heptadecanoyl chain at the *sn*-1 position (Pellegrino et al. 2014). Phospholipase A₂ (PLA₂) hydrolyses the ester bond of the fatty acyl group attached at the *sn*-2 position of PC, producing LysoPC and free fatty acid (FFA) (Farooqui et al. 2009). Alternatively, LysoPC can be converted into PC by incorporation of an acyl moiety at the *sn*-2 position of the glycerol backbone by

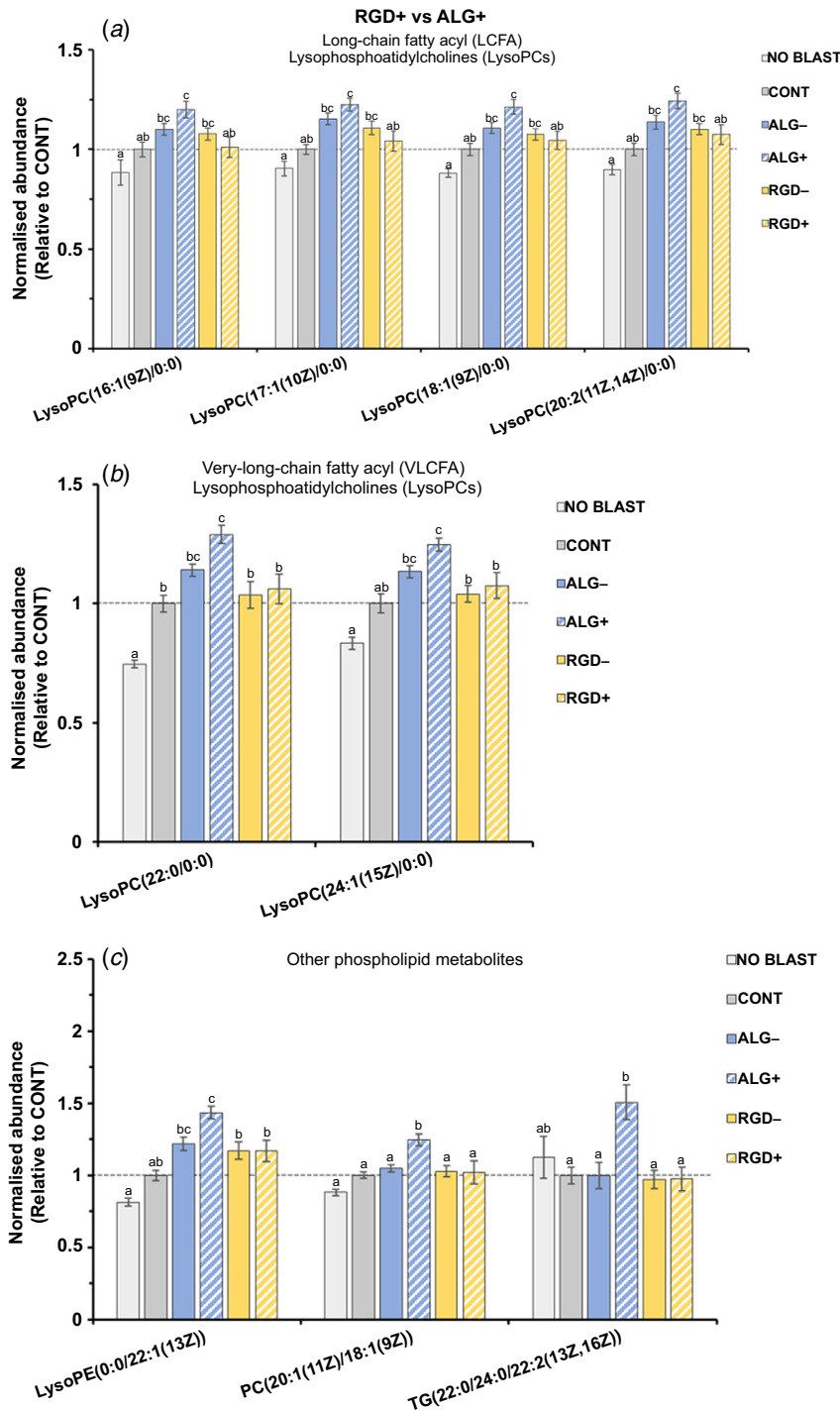


Fig. 6. Abundance differences of phospholipid metabolites within media from elongating porcine blastocysts encapsulated in unmodified alginate or RGD-alginate hydrogels. Differences ($P < 0.05$) in normalised abundance of metabolites between media collected from blastocysts initiating elongation after 96 h of culture encapsulated in RGD-alginate (RGD+) or unmodified alginate (ALG+) involved in phospholipid metabolism, including (a) long-chain fatty acyl (LCFA) lysophosphatidylcholines (LysoPCs), (b) very-long-chain fatty acyl (VLCFA) LysoPCs, and (c) other phospholipid metabolites. Bar graphs depict the influence of alginate hydrogel encapsulating blastocysts initiating elongation on the normalised abundance of the metabolites within corresponding culture media; graphs also display pairwise comparisons of normalised metabolite abundance within media from RGD+, ALG+, blastocysts encapsulated in RGD-alginate that did not initiate elongation (RGD-), blastocysts encapsulated in unmodified alginate that did not initiate elongation (ALG-), non-encapsulated, 2D culture control blastocysts (CONT), and media without cultured blastocysts (NO BLAST). Metabolite abundance values are reported as LSM \pm s.e.m. and normalised relative to CONT for each metabolite (CONT values are designated as 1, indicated by the dashed line at $y = 1$); bars with different letters differ ($P < 0.05$) for each metabolite.

LysoPC acyltransferase 1–4 (LPCAT1-4) (Zhao *et al.* 2008). These phospholipid metabolites are involved in PC biosynthesis and degradation in remodelling of the phospholipid plasma membrane. In addition to regulating cell maintenance and growth, membrane PCs play important roles in regulating membrane-associated protein activities and serve as precursors of bioactive lipids involved in intracellular signalling (Cao *et al.* 2008; Zhao *et al.* 2008;

Golczak *et al.* 2012). In addition to regulating cell maintenance and growth, membrane PCs play important roles in regulating membrane-associated protein activities and serve as precursors of bioactive lipids involved in intracellular signalling (Tafesse *et al.* 2007; Cao *et al.* 2008; Shulga *et al.* 2011; Takahashi and Suzuki 2012). During rapid elongation, the porcine conceptus undergoes remodelling of the lipid composition within the trophectoderm plasma

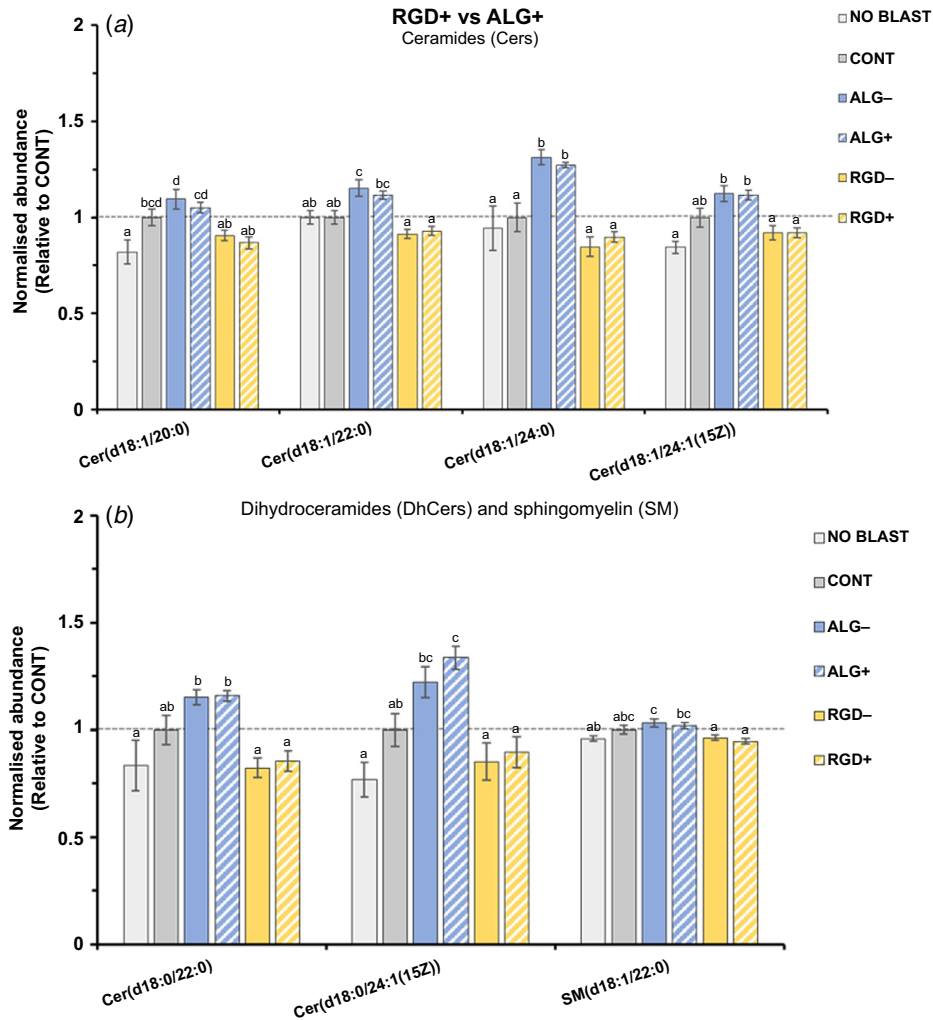


Fig. 7. Abundance differences of sphingolipid metabolites within media from elongating porcine blastocysts encapsulated in unmodified alginate and RGD-alginate hydrogels. Differences ($P < 0.05$) in normalised abundance of metabolites between media collected from blastocysts initiating elongation after 96 h of culture encapsulated in RGD-alginate (RGD+) or unmodified alginate (ALG+) involved in sphingolipid metabolism, including (a) ceramides (Cers) and (b) dihydroceramides (DhCers) and sphingomyelin (SM). Bar graphs depict the influence of alginate hydrogel encapsulating blastocysts initiating elongation on the normalised abundance of the metabolites within corresponding culture media; graphs also display pairwise comparisons of normalised metabolite abundance within media from RGD+, ALG+, blastocysts encapsulated in RGD-alginate that did not initiate elongation (RGD-), blastocysts encapsulated in unmodified alginate that did not initiate elongation (ALG-), non-encapsulated, 2D culture control blastocysts (CONT), and media without cultured blastocysts (NO BLAST). Metabolite abundance values are reported as LSM \pm s.e.m. and normalised relative to CONT for each metabolite (CONT values are designated as 1, indicated by the dashed line at $y = 1$); bars with different letters differ ($P < 0.05$) for each metabolite.

membrane (Bazer and Johnson 2014). In order to increase trophoblast membrane fluidity for the cellular movement and remodelling necessary for elongation, arachidonic acid (AA) is released from the trophoblast phospholipid plasma membrane by PLA2 stimulation (Geisert et al. 2017). In a recent global transcriptomic study characterising differential gene expression of the *in vivo* porcine conceptus as it

transitions through the initial stages of elongation, our group showed that several PLA2s and LPCAT-1 and -3 were upregulated from spherical to ovoid and/or spherical to tubular conceptus morphologies while another PLA2, phospholipase B1, and LPCAT-2 and -4 were downregulated, and all are known contributors of ether lipid metabolism and glycerophospholipid metabolism pathways (Miles et al. 2022;

Walsh *et al.* 2022). The increase in abundance of PC metabolites within the current study, combined with previously identified upregulation of genes involved in membrane phospholipid metabolism throughout the progression of elongation, suggest that PC metabolism is increased in blastocysts initiating elongation.

Within the current study, the abundance of Gb3(d18:1/16:0) was greater in culture media from ALG+ blastocysts. Trihexosylceramide is a globoside formed by the transfer of galactose (Gal) to lactosylceramide (LacCer) by LacCer 4- α -galactosyltransferase (Kok *et al.* 2021). Conversely, Gb3 can be hydrolysed by galactosidase alpha (GLA) to produce LacCer and Gal (Kok *et al.* 2021). Recently, we have shown that *GLA* is downregulated in the ovoid and tubular porcine conceptus compared to spherical within enriched glycerolipid metabolism and sphingolipid metabolism pathways (Walsh *et al.* 2022), and together with the increased Gb3 abundance in media from ALG+ blastocysts within the current study, suggests that catabolism of Gb3 may be decreased in the elongating porcine conceptus. Within the glycosphingolipid metabolism pathway, uridine diphosphate (UDP)-*N*-acetylgalactosamine (GalNAc):beta-1,3-acetylgalactosaminyltransferase 1 transfers GalNAc from UDP-GalNAc to Gb3 to produce Gb4, while beta-hexosaminidase A (HEXA) and HEXD convert Gb4 to Gb3 (Jacob *et al.* 2014; Ryckman *et al.* 2020). Beta-1,3-galactosyltransferase 5 can transfer Gal from UDP-Gal to Gb4 to produce stage-specific embryonic antigen 3 (SSEA-3) (Kuo *et al.* 2017). SSEA-3 can then be sialylated to SSEA-4 by cytidine monophosphate (CMP)-*N*-acetylneuraminyl-beta-galactosamide- α -2,3-sialyltransferase 1-2,4 (*ST3GAL1-2,4*); alternatively, galactoside α -(1,2)-fucosyltransferase 1 (*FUT1*) can catalyse fucosylation of SSEA-3 to generate Globo H (Suila *et al.* 2011; Kuo *et al.* 2017). Stage-specific embryonic antigen 3, SSEA-4, and Globo H are pluripotent and embryonic stem cell markers that have been suggested to play a role in early embryogenesis and are associated with processes such as cell recognition, adhesion, and signal transduction (Suila *et al.* 2011; Hou *et al.* 2016; Asano *et al.* 2019). Interestingly, decreased expression of *FUT1* has been detected in porcine blastocysts as they transition from spherical to ovoid and from spherical to tubular conceptus morphologies, while *ST3GAL1* and *ST3GAL4* expression increases from spherical to tubular morphology (Walsh *et al.* 2022). These gene expression changes of *FUT1*, *ST3GAL1*, and *ST3GAL4* may indicate a switch in globoside metabolism as elongation initiates and interactions between the trophoblast membrane and maternal endometrium increase through implantation (Whyte and Robson 1984; Geisert *et al.* 2015). Therefore, alterations to membrane glycosphingolipids composition throughout this developmental period may play a key role in conceptus elongation and implantation by facilitating cell migration, adhesion, and immunoregulation at the maternal–conceptus interface (Whyte and Robson 1984).

Further changes in abundance of lipid metabolites within the current study were observed in PGA2 and TXA2 in culture media from ALG+ blastocysts. In addition to increasing fluidity of the trophoblast membrane, free AA released by PLA2-stimulated cleavage of membrane phospholipids can serve as precursors for membrane phospholipids during membrane remodelling and for bioactive signalling lipids including prostanoids, such as PGs and THXs (Geisert *et al.* 2014; Hanna and Hafez 2018). Prostaglandin-endoperoxide synthase 1-2 (*PTGS1-2*) catalyses this conversion of AA to PGG2 and PGG2 to PGH2 (Barnett *et al.* 1994; Cebrián-Prats *et al.* 2019). Prostaglandin H2 can then be converted to PGE2 by PGE synthase *PTGES2-3* (Tanioka *et al.* 2000; Watanabe *et al.* 2003; Frasor *et al.* 2008), or to TXA2 by TXA synthase 1 (Matsunobu *et al.* 2013), and dehydration of PGE2 leads to PGA2, a more stable derivative that can be readily hydrolysed back to PGE2 (Watkins *et al.* 2005). Previously, *PTGS2* was found to be downregulated from spherical to ovoid and spherical to tubular porcine conceptus morphologies (Walsh *et al.* 2022). However, *PTGS2* expression and PG synthesis is known to be elevated in the maternal endometrium during porcine peri-implantation development (Ashworth *et al.* 2006; Pfeiffer *et al.* 2020). The regulation of endometrial gene expression by PGs to produce a uterine environment promoting conceptus attachment and growth is essential in the establishment and maintenance of pregnancy and early conceptus development and implantation (Geisert *et al.* 2014). Prostanoids regulate gene expression by attaching to their receptors, such as PGE receptor 1-4 (*PTGER1-4*) and TXA2 receptor (Watkins *et al.* 2005; Markosyan *et al.* 2006). In a recent study, porcine conceptus *PTGER4* expression was found to be upregulated from spherical to ovoid and spherical to tubular conceptus morphologies (Walsh *et al.* 2022). Altogether, these results support the importance of prostanoid signalling for establishing a uterine environment that promotes porcine conceptus development and elongation and potentially suggesting an autocrine or paracrine function of PGs within blastocysts as a mechanism for initiating or complementing the initiation of elongation.

Additional evidence of metabolic changes within lipid signalling pathways during the initiation of porcine conceptus elongation was the increased abundance of 17-OHP in culture media from ALG+ and RGD+ blastocysts within the current study. Our previous study showed upregulation of *CYP17A1*, as well as *STAR*, *CYP19A1*, *CYP11A1*, *hydroxysteroid 17- β dehydrogenase 1*, and *hydroxysteroid 11- β dehydrogenase 2* from spherical to ovoid and/or tubular, and downregulation of *steroid 5- α -reductase 1* from spherical to tubular, within ovarian steroidogenesis, steroid hormone biosynthesis, cortisol synthesis and secretion, and prolactin signalling pathways (Walsh *et al.* 2022). Additionally, in the uterine luminal environment throughout the initiation of porcine conceptus elongation, we identified a decrease in ULF abundance of

cholesterol from initial spherical to later ovoid and tubular elongation stages (Walsh *et al.* 2020), suggesting changes in cholesterol metabolism and steroid hormone biosynthesis during the initiation of elongation. It is well established that on days 10–12 of pregnancy in the pig, the conceptus secretes E2 to induce endometrial changes involved in mediating conceptus elongation and signalling the maternal recognition of pregnancy (Bazer and Johnson 2014; Kiewisz *et al.* 2014). Therefore, greater abundance of 17-OHP in media from ALG+ and RGD+ blastocysts within the current study, as well as the increased expression of steroidogenic genes within elongating blastocysts identified in previous studies, provides more complete support to the essential role of increased steroid hormone biosynthesis as the porcine conceptus initiates elongation.

Two metabolites involved in amino acid metabolism, (*R*)-salsolinol and 3-OH-isobutyryl-CoA, were more abundant in culture media from ALG+ and RGD+ blastocysts within the current study. (*R*)-salsolinol is a metabolite within the phenylalanine, tyrosine, and dopamine metabolism pathway (Meiser *et al.* 2013). Within this pathway, dihydroxyphenylalanine (DOPA) is converted to dopamine by DOPA decarboxylase that can be metabolised to (*R*)-salsolinol by salsolinol synthase (Chen *et al.* 2018; Kurnik-Lucka *et al.* 2018). Further evidence of changes in amino acid metabolic processes during the initiation of porcine conceptus elongation was the differential abundance of 3-OH-isobutyryl-CoA, an intermediate in the catabolism of valine (Loupatty *et al.* 2007), between media from ALG+ blastocysts and ALG– media in the current study. Conceptus metabolism of amino acids may play an important role in proper development and rapid elongation, as these compounds are involved in nucleotide and protein synthesis, molecular signalling, and cellular proliferation (Humpherson *et al.* 2005; Ross *et al.* 2009; O’Neil and Spencer 2021). Our previous *in vivo* metabolomic study identified changes in ULF abundance of phenylalanine, tyrosine, and the isoleucine catabolism by-product 2-methylbutyryl-L-carnitine, as well as metabolites of the urea cycle involved in amino acid catabolism, throughout the progression of elongation (Walsh *et al.* 2020), providing further evidence of changes in amino acid metabolism during the elongation process. Thus, the abundance increases of (*R*)-salsolinol and 3-OH-isobutyryl-CoA emphasise the important role of amino acid metabolism in processes that promote the rapid trophoblast remodelling that occurs during the initiation of porcine conceptus elongation (Humpherson *et al.* 2005).

Metabolic differences between RGD+ and RGD– blastocysts and between RGD+ and ALG+ blastocysts after 96 h of culture

The current metabolomic analyses were performed with the goal of uncovering contributions of the RGD binding motif to the initiation of porcine conceptus elongation and

identifying potential RGD-mediated metabolic mechanisms involved in this process. The RGD adhesion peptide in SPP1 has been previously identified as an important factor contributing to porcine conceptus elongation and subsequent implantation by binding to integrin receptors present on both the porcine uterine epithelium and conceptus trophoblast to facilitate trophoblast attachment, spreading, and migration, and induce cytoskeletal reorganisation and the formation of focal adhesions during conceptus elongation via adhesion at the maternal–conceptus interface (Garlow *et al.* 2002; Erikson *et al.* 2009). We have previously shown that spherical porcine blastocysts encapsulated within our RGD-alginate hydrogel culture system had increased survival compared to non-encapsulated control blastocysts and the number of blastocysts encapsulated in RGD-alginate that initiated morphological changes was higher compared to those encapsulated in unmodified alginate or non-encapsulated control blastocysts (Laughlin *et al.* 2017). Elongating blastocysts within RGD-alginate hydrogels had increased *IL1B2* gene expression compared to blastocysts encapsulated in unmodified alginate (Laughlin *et al.* 2017) presumably due to the stimulation of integrin signalling eliciting maternal–conceptus crosstalk and promoting conceptus–hydrogel matrix adhesion and cell migration (Laughlin *et al.* 2017; Miles *et al.* 2017), providing further support for the critical role of RGD-integrin binding in promoting the initiation of porcine conceptus elongation.

Within the current study, the abundance of phospholipid metabolites including LysoPC(20:3/0:0), LysoPC(20:4/0:0), LysoPC(22:4/0:0), and LysoPC(22:4/0:0) was less in media from RGD+ blastocysts. In our previous transcriptomic study, many influential genes were differentially expressed between spherical and ovoid and/or spherical and tubular conceptus morphologies within the glycerolipid and glycerophospholipid metabolism pathways (Walsh *et al.* 2022). The differential expression of these key glycerophospholipid metabolism genes demonstrates changes in the phospholipid composition of plasma membrane throughout the conceptus transition through initial elongation stages as PCs and LysoPCs within the membrane are being constantly metabolised and resynthesised into new glycerolipid and phospholipid species at different rates (Farooqui *et al.* 2009; van der Veen *et al.* 2017). Many of the lipid metabolites and products resulting from metabolism of membrane phospholipids can then be used for functions outside of modifying membrane composition (e.g. oxidation of TAGs and FFAs for energy, synthesis of bioactive lipid signalling molecules and receptors, and influence of lipid metabolism through regulation of gene expression and availability of lipid substrates and precursors) (Shulga *et al.* 2011; Ribeiro *et al.* 2016). These functions potentially affect other aspects of lipid metabolism and bioactive signalling both within the conceptus and between the conceptus and the maternal endometrium to drive elongation. The decreased abundance of LysoPCs in media from RGD+ blastocysts may indicate

that RGD-mediated elongation of porcine blastocysts involves a shift in membrane PC metabolism, specifically resulting in a decrease in conceptus release of LysoPC into the uterine luminal environment as blastocysts initiate morphological changes.

Similarly within the current study, the abundance of metabolites in phospholipid metabolism including LysoPC(16:1/0:0), LysoPC(17:1/0:0), LysoPC(18:1/0:0), LysoPC(20:2/0:0), LysoPC(22:0/0:0), LysoPC(24:1/0:0), PC(20:1/18:1), LysoPE(0:0/22:1), and TAG(22:0/24:0/22:2) was decreased in media from RGD+ blastocysts. In addition, abundance of metabolites in sphingolipid metabolism including Cer(d18:1/20:0), Cer(d18:1/22:0), Cer(d18:1/24:0), Cer(d18:1/24:1), Cer(d18:0/22:0), Cer(d18:0/24:1), and SM(d18:1/22:0) was less in media from RGD+ blastocysts. Ceramides can be incorporated into sphingolipids within cell membranes, as well as have important roles in cell signalling pathways that may regulate cell differentiation, proliferation, and synthesis of bioactive signalling lipids that is essential in guiding the initiation of conceptus elongation (O'Neil and Spencer 2021). Recently, differential expression of many key genes within the significantly enriched sphingolipid metabolism pathway was identified between spherical and ovoid and/or spherical and tubular porcine conceptus morphologies (e.g. *alkaline ceramidase 2*, *Cer kinase*, and *Cer synthases*) (Walsh *et al.* 2022). In addition, an increase in abundance of ethanolamine and hexadecaspinganine was observed in ULF throughout the progression of porcine conceptus elongation *in vivo* (Walsh *et al.* 2020), further implicating changes in phospholipid and sphingolipid metabolism associated with the initiation of elongation (Miles *et al.* 2022). The differential expression of these phospholipid and sphingolipid metabolism genes between conceptus morphologies at the initiation of elongation, combined with the decreased abundance of phospholipid and sphingolipid metabolites in media from RGD+ blastocysts, may suggest that the RGD adhesion ligand that is present during porcine conceptus elongation *in vivo* may influence the phospholipid and sphingolipid metabolism pathways and metabolite fates that serve as driving mechanisms of the initial morphological changes of elongation. Alternatively, decreased secretion of these metabolites may be due to increased stability of the trophectoderm membrane/ECM during conceptus-endometrial adhesion via RGD-integrin receptor binding, which could result in decreased release of membrane phospholipid and sphingolipid metabolites into the extra-embryonic environment. In a neuroblastoma model, inhibition of ceramide release was regulated by RGD-specific mechanisms through binding of integrin receptors (Erdreich-Epstein *et al.* 2000). Given the involvement of integrins to drive changes to the trophectoderm during porcine conceptus elongation (Erikson *et al.* 2009; Miles *et al.* 2022; Walsh *et al.* 2022), it is possible that RGD-integrin binding mechanisms within the RGD+ blastocysts may increase the stability of the

trophectoderm and surrounding ECM, resulting in the decreased release of these metabolites, and subsequently facilitate initiation of elongation.

Conclusions

The goal of this study was to characterise differences in the abundance of metabolites within the media of cultured blastocysts, encapsulated within unmodified alginate and RGD-alginate hydrogel systems that did or did not initiate morphological changes to gain more understanding of mechanisms that are essential in the initiation of porcine conceptus elongation. The current study implicated changes in phospholipid, glycosphingolipid, lipid signalling, and amino acid metabolic processes as potential RGD-independent mechanisms of elongation and decreased secretion of LysoPCs, phospholipid, and sphingolipid metabolites as potential RGD-mediated mechanisms of elongation. Further analysis of elongation mechanisms within unmodified alginate and RGD-alginate hydrogel systems to identify gene expression changes from individual blastocysts associated with the metabolite abundance differences within culture media observed in the current study may help elucidate the specific mechanisms contributing to differences in elongation characteristics between these two systems. While these results represent metabolite secretions from conceptuses undergoing initiation of elongation *in vitro*, they may not necessarily reflect the mechanisms that occur *in vivo*. Nonetheless, model systems like that used here can be important tools to guide further investigation of the mechanism of elongation.

Supplementary material

Supplementary material is available [online](#).

References

- Arnhold J, Osipov AN, Spalteholz H, Panasenkov OM, Schiller J (2002) Formation of lysophospholipids from unsaturated phosphatidylcholines under the influence of hypochlorous acid. *Biochimica et Biophysica Acta (BBA) - General Subjects* 1572(1), 91–100. doi:10.1016/S0304-4165(02)00271-4
- Asano S, Pal R, Tanaka H-N, Imamura A, Ishida H, Suzuki KGN, Ando H (2019) Development of fluorescently labeled SSEA-3, SSEA-4, and Globo-H glycosphingolipids for elucidating molecular interactions in the cell membrane. *International Journal of Molecular Sciences* 20(24), 6187–6187. doi:10.3390/IJMS20246187
- Ashworth CJ, Pickard AR, Miller SJ, Flint APF, Diehl JR (1997) Comparative studies of conceptus-endometrial interactions in Large White × Landrace and Meishan gilts. *Reproduction, Fertility and Development* 9(2), 217–226. doi:10.1071/R96040
- Ashworth MD, Ross JW, Hu J, White FJ, Stein DR, DeSilva U, Johnson GA, Spencer TE, Geisert RD (2006) Expression of porcine endometrial prostaglandin synthase during the estrous cycle and early pregnancy, and following endocrine disruption of pregnancy. *Biology of Reproduction* 74(6), 1007–1015. doi:10.1095/biolreprod.105.046557

- Barnett J, Chow J, Ives D, Chiou M, Mackenzie R, Osen E, Nguyen B, Tsing S, Bach C, Freire J, Chan H, Sigal E, Ramesha C (1994) Purification, characterization and selective inhibition of human prostaglandin G/H synthase 1 and 2 expressed in the baculovirus system. *Biochimica et Biophysica Acta (BBA) - Protein Structure and Molecular Enzymology* **1209**(1), 130–139. doi:10.1016/0167-4838(94)90148-1
- Bazer FW, Johnson GA (2014) Pig blastocyst–uterine interactions. *Differentiation* **87**(1–2), 52–65. doi:10.1016/j.diff.2013.11.005
- Bazer FW, Geisert RD, Thatcher WW, Roberts RM (1982) The establishment and maintenance of pregnancy. In 'Control of pig reproduction'. (Eds DJA Cole, GR Foxcroft) pp. 227–252. (Butterworth-Heinemann)
- Bazer FW, Thatcher WW, Martinat-Boite F, Terqui M (1988) Conceptus development in Large White and prolific Chinese Meishan pigs. *Reproduction* **84**(1), 37–42. doi:10.1530/jrf.0.0840037
- Blomberg LA, Long EL, Sonstegard TS, Van Tassell CP, Dobrinsky JR, Zuelke KA (2005) Serial analysis of gene expression during elongation of the peri-implantation porcine trophoderm (conceptus). *Physiological Genomics* **20**(2), 188–194. doi:10.1152/physiolgenomics.00157.2004
- Blomberg LA, Garrett WM, Guillomot M, Miles JR, Sonstegard TS, Van Tassell CP, Zuelke KA (2006) Transcriptome profiling of the tubular porcine conceptus identifies the differential regulation of growth and developmentally associated genes. *Molecular Reproduction and Development* **73**(12), 1491–1502. doi:10.1002/mrd.20503
- Brandão DO, Maddox-Hyttel P, Løvendahl P, Rumpf R, Stringfellow D, Callesen H (2004) Post hatching development: a novel system for extended *in vitro* culture of bovine embryos. *Biology of Reproduction* **71**(6), 2048–2055. doi:10.1095/biolreprod.103.025916
- Broeckling CD, Afsar FA, Neumann S, Ben-Hur A, Prenni JE (2014) RAMClust: a novel feature clustering method enables spectral-matching-based annotation for metabolomics data. *Analytical Chemistry* **86**(14), 6812–6817. doi:10.1021/ac501530d
- Broeckling CD, Ganna A, Layer M, Brown K, Sutton B, Ingelsson E, Peers G, Prenni JE (2016) Enabling efficient and confident annotation of LC–MS metabolomics data through MS1 spectrum and time prediction. *Analytical Chemistry* **88**(18), 9226–9234. doi:10.1021/acs.analchem.6b02479
- Cao J, Shan D, Revett T, Li D, Wu L, Liu W, Tobin JF, Gimeno RE (2008) Molecular identification of a novel mammalian brain isoform of acyl-CoA:lysophospholipid acyltransferase with prominent ethanolamine lysophospholipid acylating activity, LPEAT2. *Journal of Biological Chemistry* **283**(27), 19049–19057. doi:10.1074/jbc.M800364200
- Cebrián-Prats A, González-Lafont A, Lluçh JM (2019) Unraveling the molecular details of the complete mechanism that governs the synthesis of prostaglandin G2 catalyzed by cyclooxygenase-2. *ACS Omega* **4**(1), 2063–2074. doi:10.1021/acsomega.8b03575
- Chen X, Zheng X, Ali S, Guo M, Zhong R, Chen Z, Zhang Y, Qing H, Deng Y (2018) Isolation and sequencing of salsolinol synthase, an enzyme catalyzing salsolinol biosynthesis. *ACS Chemical Neuroscience* **9**(6), 1388–1398. doi:10.1021/acscchemneuro.8b00023
- Djombou Feunang Y, Eisner R, Knox C, Chepelev L, Hastings J, Owen G, Fahy E, Steinbeck C, Subramanian S, Bolton E, Greiner R, Wishart DS (2016) ClassyFire: automated chemical classification with a comprehensive, computable taxonomy. *Journal of Cheminformatics* **8**, 61. doi:10.1186/s13321-016-0174-y
- Erdreich-Epstein A, Shimada H, Groshen S, Liu M, Metelitsa LS, Kim KS, Stins MF, Seeger RC, Durden DL (2000) Integrins $\alpha_v\beta_3$ and $\alpha_v\beta_5$ are expressed by endothelium of high-risk neuroblastoma and their inhibition is associated with increased endogenous ceramide. *Cancer Research* **60**(3), 712–721.
- Erikson DW, Burghardt RC, Bayless KJ, Johnson GA (2009) Secreted phosphoprotein 1 (SPP1, osteopontin) binds to integrin $\alpha_v\beta_6$ on porcine trophoderm cells and integrin $\alpha_v\beta_3$ on uterine luminal epithelial cells, and promotes trophoderm cell adhesion and migration. *Biology of Reproduction* **81**(5), 814–825. doi:10.1095/biolreprod.109.078600
- Farooqui AA, Horrocks LA, Farooqui T (2009) Choline and ethanolamine glycerophospholipids. In 'Handbook of neurochemistry and molecular neurobiology'. (Eds A Lajtha, G Tettamanti, G Goracci) pp. 21–38. (Springer: Boston, MA)
- FASS (2010) 'Guide for care and use of agricultural animals in research and teaching.' 3rd edn. (FASS: Champaign, IL)
- Frasor J, Weaver AE, Pradhan M, Mehta K (2008) Synergistic up-regulation of prostaglandin E synthase expression in breast cancer cells by 17 β -estradiol and proinflammatory cytokines. *Endocrinology* **149**(12), 6272–6279. doi:10.1210/en.2008-0352
- Garlow JE, Ka H, Johnson GA, Burghardt RC, Jaeger LA, Bazer FW (2002) Analysis of osteopontin at the maternal-placental interface in pigs. *Biology of Reproduction* **66**(3), 718–725. doi:10.1095/biolreprod66.3.718
- Geisert RD, Schmitt RAM (2002) Early embryonic survival in the pig: can it be improved? *Journal of Animal Science* **80**(E-Suppl_1), E54–E65.
- Geisert RD, Renegar RH, Thatcher WW, Roberts RM, Bazer FW (1982) Establishment of pregnancy in the pig: I. Interrelationships between preimplantation development of the pig blastocyst and uterine endometrial secretions. *Biology of Reproduction* **27**(4), 925–939. doi:10.1095/biolreprod27.4.925
- Geisert RD, Lucy MC, Whyte JJ, Ross JW, Mathew DJ (2014) Cytokines from the pig conceptus: roles in conceptus development in pigs. *Journal of Animal Science and Biotechnology* **5**, 51. doi:10.1186/2049-1891-5-51
- Geisert RD, Johnson GA, Burghardt RC (2015) Implantation and establishment of pregnancy in the pig. In 'Regulation of implantation and establishment of pregnancy in mammals: tribute to 45 year anniversary of Roger V. Short's "maternal recognition of pregnancy". Vol. 216'. (Eds RD Geisert, FW Bazer) pp. 137–163. (Springer: Cham, Switzerland)
- Geisert RD, Whyte JJ, Meyer AE, Mathew DJ, Juárez MR, Lucy MC, Prather RS, Spencer TE (2017) Rapid conceptus elongation in the pig: an interleukin 1 beta 2 and estrogen-regulated phenomenon. *Molecular Reproduction and Development* **84**(9), 760–774. doi:10.1002/mrd.22813
- Golczak M, Kiser PD, Sears AE, Lodowski DT, Blaner WS, Palczewski K (2012) Structural basis for the acyltransferase activity of lecithin: retinol acyltransferase-like proteins. *Journal of Biological Chemistry* **287**(28), 23790–23807. doi:10.1074/jbc.M112.361550
- Hanna VS, Hafez EAA (2018) Synopsis of arachidonic acid metabolism: a review. *Journal of Advanced Research* **11**, 23–32. doi:10.1016/j.jare.2018.03.005
- Hou D-R, Jin Y, Nie X-W, Zhang M-L, Ta N, Zhao L-H, Yang N, Chen Y, Wu Z-Q, Jiang H-B, Li Y-R, Sun Q-Y, Dai Y-F, Li R-F (2016) Derivation of porcine embryonic stem-like cells from *in vitro*-produced blastocyst-stage embryos. *Scientific Reports* **6**(1), 25838. doi:10.1038/srep25838
- Humpherson PG, Leese HJ, Sturmey RG (2005) Amino acid metabolism of the porcine blastocyst. *Theriogenology* **64**(8), 1852–1866. doi:10.1016/j.theriogenology.2005.04.019
- Jacob F, Hitchins MP, Fedier A, Brennan K, Nixdorf S, Hacker NF, Ward R, Heinzlmann-Schwarz VA (2014) Expression of *GBGT1* is epigenetically regulated by DNA methylation in ovarian cancer cells. *BMC Molecular Biology* **15**(1), 24. doi:10.1186/1471-2199-15-24
- Jaeger C, Méret M, Schmitt CA, Lisec J (2017) Compound annotation in liquid chromatography/high-resolution mass spectrometry based metabolomics: robust adduct ion determination as a prerequisite to structure prediction in electrospray ionization mass spectra. *Rapid Communications in Mass Spectrometry* **31**(15), 1261–1266. doi:10.1002/rcm.7905
- Kiewisz J, Krawczynski K, Lisowski P, Blitek A, Zwierzchowski L, Ziecik AJ, Kaczmarek MM (2014) Global gene expression profiling of porcine endometria on Days 12 and 16 of the estrous cycle and pregnancy. *Theriogenology* **82**(6), 897–909. doi:10.1016/j.theriogenology.2014.07.009
- Kim S, Thiessen PA, Cheng T, Zhang J, Gindulyte A, Bolton EE (2019) PUG-View: programmatic access to chemical annotations integrated in PubChem. *Journal of Cheminformatics* **11**(1), 56. doi:10.1186/s13321-019-0375-2
- Kok K, Zwiers KC, Boot RG, Overkleeft HS, Aerts JMFG, Artola M (2021) Fabry disease: molecular basis, pathophysiology, diagnostics and potential therapeutic directions. *Biomolecules* **11**(2), 271–271. doi:10.3390/biom11020271
- Kuo H-H, Lin R-J, Hung J-T, Hsieh C-B, Hung T-H, Lo F-Y, Ho M-Y, Yeh C-T, Huang Y-L, Yu J, Yu AL (2017) High expression *FUT1* and *B3GALT5* is an independent predictor of postoperative recurrence and survival in hepatocellular carcinoma. *Scientific Reports* **7**, 10750. doi:10.1038/s41598-017-11136-w

- Kurnik-Lucka M, Panula P, Bugajski A, Gil K (2018) Salsolinol: an unintelligible and double-faced molecule – lessons learned from *in vivo* and *in vitro* experiments. *Neurotoxicity Research* **33**(2), 485–514. doi:10.1007/s12640-017-9818-6
- Laughlin TD, Miles JR, Wright-Johnson EC, Rempel LA, Lents CA, Pannier AK (2017) Development of pre-implantation porcine blastocysts cultured within alginate hydrogel systems either supplemented with secreted phosphoprotein 1 or conjugated with Arg-Gly-Asp Peptide. *Reproduction, Fertility and Development* **29**(12), 2345–2356. doi:10.1071/RD16366
- Liebisch G, Vizcaíno JA, Köfeler H, Trötzmüller M, Griffiths WJ, Schmitz G, Spener F, Wakelam MJO (2013) Shorthand notation for lipid structures derived from mass spectrometry. *Journal of Lipid Research* **54**(6), 1523–1530. doi:10.1194/jlr.M033506
- Loupatty FJ, Clayton PT, Ruitter JPN, Ofman R, Ijlst L, Brown GK, Thorburn DR, Harris RA, Duran M, DeSousa C, Krywawych S, Heales SJR, Wanders RJA (2007) Mutations in the gene encoding 3-hydroxyisobutyryl-CoA hydrolase results in progressive infantile neurodegeneration. *The American Journal of Human Genetics* **80**(1), 195–199. doi:10.1086/510725
- Markosyan N, Dozier BL, Lattanzio FA, Duffy DM (2006) Primate granulosa cell response via prostaglandin E2 receptors increases late in the periovulatory interval. *Biology of Reproduction* **75**(6), 868–876. doi:10.1095/biolreprod.106.053769
- Matsunobu T, Okuno T, Yokoyama C, Yokomizo T (2013) Thromboxane A synthase-independent production of 12-hydroxyheptadecatrienoic acid, a BLT2 ligand. *Journal of Lipid Research* **54**(11), 2979–2987. doi:10.1194/jlr.M037754
- Meiser J, Weindl D, Hiller K (2013) Complexity of dopamine metabolism. *Cell Communication and Signaling* **11**(1), 34. doi:10.1186/1478-811X-11-34
- Miles JR, Freking BA, Blomberg LA, Vallet JL, Zuelke KA (2008) Conceptus development during blastocyst elongation in lines of pigs selected for increased uterine capacity or ovulation rate. *Journal of Animal Science* **86**(9), 2126–2134. doi:10.2527/jas.2008-1066
- Miles JR, Laughlin TD, Sargus-Patino CN, Pannier AK (2017) *In vitro* porcine blastocyst development in three-dimensional alginate hydrogels. *Molecular Reproduction and Development* **84**(9), 775–787. doi:10.1002/mrd.22814
- Miles JR, Walsh SC, Rempel LA, Pannier AK (2022) Mechanisms regulating the initiation of porcine conceptus elongation. *Molecular Reproduction and Development*. doi:10.1002/mrd.23623
- O’Neil EV, Spencer TE (2021) Insights into the lipidome and primary metabolome of the uterus from day 14 cyclic and pregnant sheep. *Biology of Reproduction* **105**(1), 87–99. doi:10.1093/biolre/iaob053
- Pellegrino RM, Di Veroli A, Valeri A, Goracci L, Cruciani G (2014) LC/MS lipid profiling from human serum: a new method for global lipid extraction. *Analytical and Bioanalytical Chemistry* **406**(30), 7937–7948. doi:10.1007/s00216-014-8255-0
- Pfeiffer CA, Meyer AE, Brooks KE, Chen PR, Milano-Foster J, Spate LD, Benne JA, Cecil RF, Samuel MS, Ciernia LA, Spinka CM, Smith MF, Wells KD, Spencer TE, Prather RS, Geisert RD (2020) Ablation of conceptus PTGS2 expression does not alter early conceptus development and establishment of pregnancy in the pig. *Biology of Reproduction* **102**(2), 475–488. doi:10.1093/biolre/ioz192
- PigCHAMP (2020) USA 2020 – year end summary. Available at <https://www.pigchamp.com/news/benchmark-magazine/articles/usa-2020-year-summary>. (Vol. 2021)
- Pope WF (1994) Embryonic mortality in swine. In ‘Embryonic mortality in domestic animals’. (Eds MT Zavy, RD Geisert) pp. 53–77. (CRC Press: Boca Raton, FL)
- Pope WF, First NL (1985) Factors affecting the survival of pig embryos. *Theriogenology* **23**(1), 91–105. doi:10.1016/0093-691X(85)90075-5
- Ribeiro ES, Greco LF, Bisinotto RS, Lima FS, Thatcher WW, Santos JE (2010) Biology of preimplantation conceptus at the onset of elongation in dairy cows. *Biology of Reproduction* **94**(4), 1–18. doi:10.1095/biolreprod.115.134908
- Ross JW, Ashworth MD, Stein DR, Couture OP, Tuggle CK, Geisert RD (2009) Identification of differential gene expression during porcine conceptus rapid trophoblastic elongation and attachment to uterine luminal epithelium. *Physiological Genomics* **36**(3), 140–148. doi:10.1152/physiolgenomics.00022.2008
- Rowley JA, Madlambayan G, Mooney DJ (1999) Alginate hydrogels as synthetic extracellular matrix materials. *Biomaterials* **20**(1), 45–53. doi:10.1016/S0142-9612(98)00107-0
- Ryckman AE, Brockhausen I, Walia JS (2020) Metabolism of glycosphingolipids and their role in the pathophysiology of lysosomal storage disorders. *International Journal of Molecular Sciences* **21**(18), 6881–6881. doi:10.3390/ijms21186881
- Sargus-Patino CN, Wright EC, Plautz SA, Miles JR, Vallet JL, Pannier AK (2014) *In vitro* development of preimplantation porcine embryos using alginate hydrogels as a three-dimensional extracellular matrix. *Reproduction, Fertility and Development* **26**(7), 943–953. doi:10.1071/RD13008
- Shulga YV, Topham MK, Epan RM (2011) Regulation and functions of diacylglycerol kinases. *Chemical Reviews* **111**(10), 6186–6208. doi:10.1021/cr1004106
- Smith CA, Want EJ, O’Maille G, Abagyan R, Siuzdak G (2006) XCMS: processing mass spectrometry data for metabolite profiling using nonlinear peak alignment, matching, and identification. *Analytical Chemistry* **78**(3), 779–787. doi:10.1021/ac051437y
- Suila H, Pitkänen V, Hirvonen T, Heiskanen A, Anderson H, Laitinen A, Natunen S, Miller-Podraza H, Satomaa T, Natunen J, Laitinen S, Valmu L (2011) Are globoseries glycosphingolipids SSEA-3 and -4 markers for stem cells derived from human umbilical cord blood? *Journal of Molecular Cell Biology* **3**(2), 99–107. doi:10.1093/jmcb/mjq041
- Sumner LW, Amberg A, Barrett D, Beale MH, Beger R, Daykin CA, Fan TW-M, Fiehn O, Goodacre R, Griffin JL, Hankemeier T, Hardy N, Harnly J, Higashi R, Kopka J, Lane AN, Lindon JC, Marriott P, Nicholls AW, Reilly MD, Thaden JJ, Viant MR (2007) Proposed minimum reporting standards for chemical analysis: Chemical Analysis Working Group (CAWG) Metabolomics Standards Initiative (MSI). *Metabolomics* **3**(3), 211–221. doi:10.1007/s11306-007-0082-2
- Tafesse FG, Huitema K, Hermansson M, van der Poel S, van den Dikkenberg J, Uphoff A, Somerharju P, Holthuis JCM (2007) Both sphingomyelin synthases SMS1 and SMS2 are required for sphingomyelin homeostasis and growth in human HeLa cells. *Journal of Biological Chemistry* **282**(24), 17537–17547. doi:10.1074/jbc.M702423200
- Takahashi T, Suzuki T (2012) Role of sulfatide in normal and pathological cells and tissues. *Journal of Lipid Research* **53**(8), 1437–1450. doi:10.1194/jlr.R026682
- Tanioka T, Nakatani Y, Semmyo N, Murakami M, Kudo I (2000) Molecular identification of cytosolic prostaglandin E₂ synthase that is functionally coupled with cyclooxygenase-1 in immediate prostaglandin E₂ biosynthesis. *Journal of Biological Chemistry* **275**(42), 32775–32782. doi:10.1074/jbc.M003504200
- Tautenhahn R, Böttcher C, Neumann S (2008) Highly sensitive feature detection for high resolution LC/MS. *BMC Bioinformatics* **9**, 504. doi:10.1186/1471-2105-9-504
- Tsugawa H, Kind T, Nakabayashi R, Yukihira D, Tanaka W, Cajka T, Saito K, Fiehn O, Arita M (2016) Hydrogen rearrangement rules: computational MS/MS fragmentation and structure elucidation using MS-FINDER software. *Analytical Chemistry* **88**(16), 7946–7958. doi:10.1021/acs.analchem.6b00770
- van der Veen JN, Kennelly JP, Wan S, Vance JE, Vance DE, Jacobs RL (2017) The critical role of phosphatidylcholine and phosphatidylethanolamine metabolism in health and disease. *Biochimica et Biophysica Acta (BBA) - Biomembranes* **1859**(9), 1558–1572. doi:10.1016/j.bbmem.2017.04.006
- Vinsky MD, Novak S, Dixon WT, Dyck MK, Foxcroft GR (2006) Nutritional restriction in lactating primiparous sows selectively affects female embryo survival and overall litter development. *Reproduction, Fertility and Development* **18**(3), 347–355. doi:10.1071/RD05142
- Waclawik A, Kaczmarek MM, Blitek A, Kaczynski P, Ziecik AJ (2017) Embryo-maternal dialogue during pregnancy establishment and implantation in the pig. *Molecular Reproduction and Development* **84**(9), 842–855. doi:10.1002/mrd.22835
- Walsh SC, Miles JR, Yao L, Broeckling CD, Rempel LA, Wright-Johnson EC, Pannier AK (2020) Metabolic compounds within the porcine uterine environment are unique to the type of conceptus present during the early stages of blastocyst elongation. *Molecular Reproduction and Development* **87**(1), 174–190. doi:10.1002/mrd.23306

- Walsh SC, Miles JR, Keel BN, Rempel LA, Wright-Johnson EC, Lindholm-Perry AK, Oliver WT, Pannier AK (2022) Global analysis of differential gene expression within the porcine conceptus transcriptome as it transitions through spherical, ovoid, and tubular morphologies during the initiation of elongation. *Molecular Reproduction and Development* **89**(4), 175–201. doi:10.1002/mrd.23553
- Watanabe K, Ohkubo H, Niwa H, Tanikawa N, Koda N, Ito S, Ohmiya Y (2003) Essential ¹¹⁰Cys in active site of membrane-associated prostaglandin E synthase-2. *Biochemical and Biophysical Research Communications* **306**(2), 577–581. doi:10.1016/S0006-291X(03)01025-8
- Watkins G, Douglas-Jones A, Mansel RE, Jiang WG (2005) Expression of thromboxane synthase, TBXAS1 and the thromboxane A2 receptor, TBXA2R, in human breast cancer. *International Seminars in Surgical Oncology* **2**(1), 23. doi:10.1186/1477-7800-2-23
- Whyte A, Robson T (1984) Saccharides localized by fluorescent lectins on trophoblast and endometrium prior to implantation in pigs, sheep and equids. *Placenta* **5**(6), 533–540. doi:10.1016/S0143-4004(84)80007-7
- Yelich JV, Pomp D, Geisert RD (1997) Ontogeny of elongation and gene expression in the early developing porcine conceptus. *Biology of Reproduction* **57**(5), 1256–1265. doi:10.1095/biolreprod57.5.1256
- Zhao Y, Chen Y-Q, Bonacci TM, Bredt DS, Li S, Bensch WR, Moller DE, Kowala M, Konrad RJ, Cao G (2008) Identification and characterization of a major liver lysophosphatidylcholine acyltransferase. *Journal of Biological Chemistry* **283**(13), 8258–8265. doi:10.1074/jbc.M710422200

Data availability. All data used to generate the results in the paper are available in the supplement tables.

Conflicts of interest. The authors declare that there are no conflicts of interest.

Declaration of funding. This study was supported by USDA-NIFA-AFRI Grant Number 2017-67015-26456 and USDA-ARS, CRIS Project 3400-31000-095-00D.

Acknowledgements. The authors would like to thank Shanda Watts, Mike Judy, and Dave Sypherd for technical assistance in collecting blastocysts, the USMARC swine crew for animal husbandry, the USMARC abattoir crew for assistance with harvesting gilts, Amber Moody for secretarial assistance, and Dr. Mark Boggess and Dr. Clay Lents for critical review of the manuscript. Mention of trade names is necessary to report factually on available data; however, the USDA neither guarantees nor warrants the standard of the product, and the same by USDA implies no approval of the product to the exclusion of others that may also be suitable. The USDA prohibits discrimination in all its programs and activities on the basis of race, color, national origin, age, disability, and where applicable, sex, marital status, familial status, parental status, religion, sexual orientation, genetic information, political beliefs, reprisal, or because all or part of an individual's income is derived from any public assistance program. (Not all prohibited bases apply to all programs.) Persons with disabilities who require alternative means for communication of program information (Braille, large print, audiotape, etc.) should contact USDA's TARGET Center at (202) 720-2600 (voice and TDD). To file a complaint of discrimination, write to USDA, Director, Office of Civil Rights, 1400 Independence Avenue, S.W., Washington, D.C. 20250-9410, or call (800) 795-3272 (voice) or (202) 720-6382 (TDD). USDA is an equal opportunity provider and employer.

Author affiliations

^ADepartment of Biological Systems Engineering, University of Nebraska-Lincoln, P.O. Box 830726, Lincoln, NE 68583, USA.

^BUSDA, U.S. Meat Animal Research Center, P.O. Box 166, Clay Center, NE 68933, USA.

^CBioanalysis and Omics Center, Colorado State University, Fort Collins, CO, USA.